AFRL-VA-WP-TR-2006-3012

ANALYSIS AND SUPPORT INITIATIVE FOR STRUCTURAL TECHNOLOGY (ASIST)

Delivery Order 0018: Active Vibration Control of Buffet-Induced Vibrations in the Vertical Tail of F/A-18

Saythia Hanagud
Patrick Roberts

Georgia Institute of Technology
The School of Aerospace Engineering
Atlanta, GA 30332-0150

JUNE 2005

Final Report for 06 June 2000 – 31 May 2005

Approved for public release; distribution is unlimited.

STINFO FINAL REPORT

AIR VEHICLES DIRECTORATE
AIR FORCE MATERIEL COMMAND
AIR FORCE RESEARCH LABORATORY
WRIGHT-PATTERSON AIR FORCE BASE, OH 45433-7542

NOTICE

Using Government drawings, specifications, or other data included in this document for any purpose other than Government procurement does not in any way obligate the U.S. Government. The fact that the Government formulated or supplied the drawings, specifications, or other data does not license the holder or any other person or corporation; or convey any rights or permission to manufacture, use, or sell any patented invention that may relate to them.

This report was cleared for public release by the Air Force Research Laboratory Wright Site (AFRL/WS) Public Affairs Office (PAO) and is releasable to the National Technical Information Service (NTIS). It will be available to the general public, including foreign nationals.

PAO Case Number: AFRL/WS-06-1414, 2 June 2006.

THIS TECHNICAL REPORT IS APPROVED FOR PUBLICATION.

/s/

DOUGLAS A. HENDERSON
Senior Aerospace Engineer
Analytical Mechanics Branch

/s/

KRISTINA LANGER, Ph.D.
Chief, Analytical Mechanics Branch
Structures Division

/s/

DAVID M. PRATT, Ph.D.
Technical Advisor
Structures Division

This report is published in the interest of scientific and technical information exchange and its publication does not constitute the Government's approval or disapproval of its ideas or findings.

REPORT DOCUMENTATION PAGE

Form Approved
OMB No. 0704-0188

1. REPORT DATE *(DD-MM-YY)*	2. REPORT TYPE	3. DATES COVERED *(From - To)*
June 2005	Final	06/06/2000– 05/31/2005

4. TITLE AND SUBTITLE
ANALYSIS AND SUPPORT INITIATIVE FOR STRUCTURAL TECHNOLOGY (ASIST)
Delivery Order 0018: Active Vibration Control of Buffet-Induced Vibrations in the Vertical Tail of F/A-18

5a. CONTRACT NUMBER
F33615-98-D-3210-0018

5b. GRANT NUMBER

5c. PROGRAM ELEMENT NUMBER
0602201

6. AUTHOR(S)
Saythia Hanagud
Patrick Roberts

5d. PROJECT NUMBER
A03J

5e. TASK NUMBER

5f. WORK UNIT NUMBER
0B

7. PERFORMING ORGANIZATION NAME(S) AND ADDRESS(ES)
Georgia Institute of Technology
The School of Aerospace Engineering
Atlanta, GA 30332-0150

8. PERFORMING ORGANIZATION REPORT NUMBER

9. SPONSORING/MONITORING AGENCY NAME(S) AND ADDRESS(ES)
Air Vehicles Directorate
Air Force Research Laboratory
Air Force Materiel Command
Wright-Patterson Air Force Base, OH 45433-7542

10. SPONSORING/MONITORING AGENCY ACRONYM(S)
AFRL-VA-WP

11. SPONSORING/MONITORING AGENCY REPORT NUMBER(S)
AFRL-VA-WP-TR-2006-3012

12. DISTRIBUTION/AVAILABILITY STATEMENT
Approved for public release; distribution is unlimited. PAO case number: AFRL/WS-06-1414, 2 June 2006.

13. SUPPLEMENTARY NOTES
Report contains color.

14. ABSTRACT (*Maximum 200 Words)*

Active controllers are designed and validated to control buffet-induced vibrations in the vertical tails of F/A-18 aircraft during high angle of attack (AOA) maneuvers. First, a procedure is developed to design the offset piezoceramic actuator assemblies, the number of actuators needed, the location of actuators, and the operational power to achieve the needed control authority. The design is limited by the specification of the worst buffet scenario that has been observed during high AOA maneuvers. Using a 1/12th scale wind tunnel model, we validated the designed controllers. The wind tunnel model is built so that the empennage is aeroelastically scaled. Adaptive neural network-based controllers are used to augment the linear controller. The adaptive neural network controls uncertainties due to parameter changes that the linear controller could not control. However, the linear controller provides the major part of the needed control authority and gives the adaptive neural network direction as to what is to be controlled.

15. SUBJECT TERMS
piezoceramic, vibration, buffet, control, damping, neural networks, aeroelasticity

16. SECURITY CLASSIFICATION OF:			17. LIMITATION OF ABSTRACT:	18. NUMBER OF PAGES	19a. NAME OF RESPONSIBLE PERSON (Monitor)
a. REPORT	b. ABSTRACT	c. THIS PAGE			Douglas A. Henderson
Unclassified	Unclassified	Unclassified	SAR	54	19b. TELEPHONE NUMBER *(Include Area Code)* (937) 904-6777

Standard Form 298 (Rev. 8-98)
Prescribed by ANSI Std. Z39-18

TABLE OF CONTENTS

Section **Page**

LIST OF FIGURES

Figures **Page**

LIST OF TABLES

Tables **Page**

FOREWORD

This report was prepared to summarize the work sponsored by the Analytical Mechanics Branch, Structures Division, Air Vehicles Directorate, Air Force Research Laboratory, Wright-Patterson Air Force Base, Ohio. The project manager was Mr. Douglas A. Henderson. The work was performed by the Georgia Institute of Technology under a delivery order contract number F33615-98-D-3210, delivery order 0018 with Anteon Corporation. The period of performance was from 6 June 2000 to 31 May 2005. Mr. Michael Gromosiak, Anteon Corp., was the contract monitor. Dr. Saythia Hanagud, Georgia Institute of Technology, School of Aerospace Engineering, was the principal investigator.

1.0 Objective

During high angle-of-attack (AOA) maneuvers, several twin-tail aircraft have encountered fin buffet[12,64,17,24]. The specific aircraft that have experienced fin buffet are F-15, F-14, F/A-18, and Eurofighter[66]. However, the buffet is not restricted only to twin tail aircraft. It has also been observed in aircraft with single, centerline vertical stabilizers. The unsteady vortices, emanating from the wing leading edge where it connects to the fuselage, impinge on the fins and induce oscillatory aerodynamic loads[15,70]. A coupling of these unsteady aerodynamic loads and the fin structure results in tail buffet[12,64,17,24]. Some consequences of buffeting are the premature initiation of fatigue cracks. Initiation and growth of these fatigue cracks result in more frequent inspections of the aircraft and additional repairs or replacement of vertical tails. During early operational deployment of F-15 and F/A-18, fatigue cracks were observed in vertical tails shortly after the aircraft were in operation. Corrective actions, at that time, consisted of strengthening the vertical tail structure by local stiffening of the structure and the use small fences at F/A-18 leading edge extensions[13,16,74,71] to reduce buffet loads. These corrective actions were not always effective in eliminating the initiation of fatigue cracks in the tail structural assembly. Following the local strengthening of the structure, the fatigue cracks moved toward different regions of the vertical tail assembly. Other passive structural control techniques are reported in references [56] and [57]. More recently[64,17,24,31,44,32,45,49,20,46,43,48,55,66], active structural control techniques have been proposed to control vibrations resulting from oscillatory loads on the empennage due to buffet. From studies, to date, on active vibration control, it can be inferred that the control authority needed for an effective vibration control is an important issue[64,17,31,32,20]. In reference [64], an offset piezoceramic stack actuator (OPSA) was proposed. The concept of the OPSA is based on the use of a larger piezoelectric coefficient d_{33} of the piezoceramic material and two optional actuator assembly parameters, i.e., the offset h and the span length L. In reference [64], the effectiveness of OPSA to deliver the needed control authority to attenuate buffet-induced vibrations of the twin vertical tails is demonstrated through wind tunnel tests on a 1/16th-scaled model of the F-15 aircraft at high AOA. However, the analysis of control authority and the design of the actuator, [64], are by a trial-and-error procedure with tests.

The objective of this project is to develop a systematic procedure to design the OPSA parameters and the controller parameters, to design the optimal placement of sensors and actuators, and to control buffet-induced vibrations. The objective of the design is to deliver the needed control authority to reduce the buffet-induced vertical tail vibrations during high AOA maneuvers. The design procedure includes the design of the actuator assembly parameters of OPSA, selection of available commercial piezoceramic stacks, and the number of needed piezoceramic stacks for a specified performance, for a specified worst-buffet scenario. The design procedure starts with a structural dynamic model for the closed loop system.

2.0 Vertical Tail Buffet Background

2.1 Control of Buffet-Induced Vibration

Even though passive approaches to tail buffet have contributed to the reduction of damage due to tail buffet, they do not reduce the damage enough to completely solve the problem and they can adjust to control multiple vibration modes. Also, passive systems can add much more weight to the tail structure than active solutions. Therefore, active solutions are sought as a solution to alleviate tail buffet fatigue damage.

In 1993, Bean[7] used tangential leading edge blowing (TLEB) in the wind tunnel on a single vertical tail to reduce buffeting. They found this was only effective at low AOA and, in fact, did not eliminate but moved the excitation and response to higher AOA. In that same year, Ashley[10,13] considered the tail buffeting as nearly linear both structurally and aerodynamically. He found that the power spectral densities and the cross spectral densities of the buffet pressure loading on the vertical tail, being quadratic functions, are directly proportional to q^2_∞. The most severe buffet on the F/A-18 occurs at $\alpha = 32°$ and 300 psf dynamic pressure. In an active approach, Ashley primarily used the rudder as the effector on the F/A-18 to reduce the magnitude of the transfer function between the pressure differential of the two sides of the vertical tail and auto power spectra of the rudder bending moment. A small control vane was attempted but failed because of the close clearance between the vertical tail and elevators on aircraft carriers. Sensing was in the form of accelerometers and this acceleration, multiplied by a gain, was directly fed back to control rudder angle, which reduced the root mean squared (RMS) level of the bending moment. This control scheme produced a 33 percent reduction in RMS moment. Two of the drawbacks of this control scheme are the reaction time of the rudder due to physical constraints and the control scheme being ineffective at lower frequencies than it is at higher frequencies. This same control scheme was applied to the F-15 at worst-case buffet conditions of $\alpha = 22°$ and 245 psf. In this case, not only did this not reduce the RMS response, but also, instabilities set in.

In the last decade, piezoelectric actuators have received an increased amount of interest due to their high efficiency in the area of active vibration control. Piezoelectric elements have a large energy density which can provide large amounts of force using very little power (less than 100 volts). In structures, these actuators can induce forces and moments that are proportional to the voltage applied across them. A large number of designs of these actuators have been developed during the past few years. In 1992, Preumont[6] reported about actuators using piezoceramic stacks that have been developed for vibration control.

Lazarus et al.[17] in 1995 performed a numerical study to assess the effectivity of piezoelectric actuators and Linear Quadratic Gaussian (LQG) control to reduce tail buffet vibrations in an F/A-18 tail. These modeled actuators were placed inside the tail skin at high strain locations. Each actuator can induce as much as 200 μstrains showing the need for multiple actuators. This model was highly detailed in that it included the plant model, structural dynamics, homogeneous aerodynamics, unsteady aerodynamic forces, sensors dynamics, actuators, anti-aliasing filters, and amplifiers. Actual flight data was used to evaluate the effectivity of this control scheme. The added weight of this system would be approximately 23 pounds. This modeling also shows that structural dynamics are only marginally changed with this active system. The added damping from this system was as much as 5.8 percent for the first mode (bending). The results showed a greater than 50 percent reduction in RMS strain and greater than 60 percent increase in damping

in the first mode was realized for less than an 8 percent increase in weight. In 1996, Moore[24] used over 100 piezoceramic wafers bonded to the inside of the vertical tail skin to achieve a 57 percent reduction in worst-case buffet conditions. A high percentage of the strain in the vertical tail during these buffet-induced vibrations is in the skin, which makes this solution very appealing. Sensing was in the form of strain gage rosette's and the control scheme was a multi-input-multi-output (MIMO) LQG. The issues with this solution are the difficult installation of the actuators and sensors. If an actuator is to be removed, it can damage the stiffened surfaces. Hauch[20] developed an active vertical tail (AVT), which successfully reduced the buffet response of structures by utilizing piezoelectric actuators, strain gauge sensors, and simple control techniques. The AVT was a 5 percent-scale aeroelastically tailored structure with twin vertical tails that exhibited vibration response similar to a full-scale aircraft structure, and was designed such that its piezoelectric actuators could provide control authority in the first two bending modes. Piezoceramic wafers were installed on the vertical tail spars. The AVT was wind-tunnel tested on a generic twin-tailed double-delta fighter model at AOA and dynamic pressures representative of actual aircraft flight envelopes including -25 to 65° AOA. At AOA, the models leading-edge vortices impinge upon the AVT. Simple control algorithms were used with piezoelectric actuators and collocated strain gauge sensors to either minimize the acceleration at the AVTs tip or the strain at the root of the tail. Control gains were verified to be a nonlinear function of AOA, dynamic pressure, and location of the actuator and sensor pair. The power spectral density (PSD) showed a 65 percent decrease in vibrations. The RMS response below 200 Hz was reduced by over 20 percent.

In 1996, Young[28] used piezoceramic stacks as force inducing actuators in truss elements and for vibration reduction in plates by placing the stack between a stiffener and the plate. In 1997, Redmond[34] used these type of actuators as moment inducing actuators by placing the stack within cutouts in stiff beams and plates (see Figure 1).

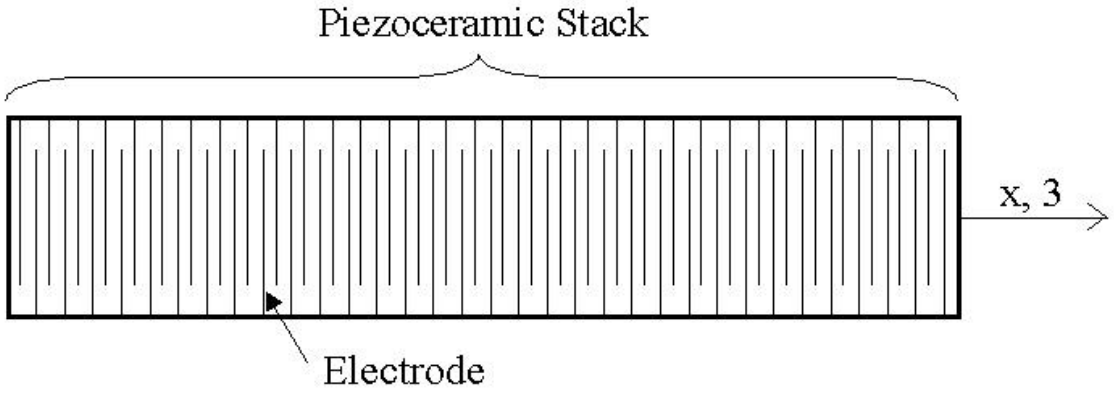

Figure 1: Co-fired Piezoceramic Stack Configuration

Active damping systems using piezoelectric elements have been modeled with finite element models (FEM) with good results. In 1996, Varadan[27] used FEM methods to obtain stresses around the bonding edges of piezoelectric wafer elements bonded to a beam. This work has shown that stresses at the bond edges and in the structure in the vicinity of the piezoelectric elements can be significant[35].

In 1997 Nitzsche et al.[32,45,61] used an aeroelastic model to evaluate two different active control strategies for tail buffet alleviation. These two methods were the active rudder approach mentioned before and a new smart structures strain actuation approach. This model included plunge, airfoil, and flap rotation, which was analogous to a vertical tail. This was augmented to

incorporate the unsteady air loads due to motion, and an internal buffet mode to simulate the buffeting excitation observed in wind tunnel tests of the vertical tail at a given range of reduced frequencies. The two control strategies that were studied used the LQG method of the Optimum Control Theory. Because active rudder has only been shown to reduce vibrations in the lower frequency range the active control system showed overall better performance as it could alleviate vibrations from low to high vibration modes.

In 1997, Moses[31], as part of the Actively Controlled Response of Buffet Affected Tails (ACROBAT) program, used a 1/16th scale model of an F/A-18 to compare two types of actuators for active damping of buffet vibrations; 1) an active rudder and 2) piezoelectric actuators. When controlling vibrations at the first bending mode using simple gain in a single-input-single-output (SISO) control scheme, the piezoelectric actuators reduced vibrations up to 60 percent at 37^{o} AOA. In 1999, Suleman[48] also used piezoceramic wafers for sensing and actuation on a sweptback flat wing model. They placed wafers at the root of the wing to add structural damping and at the wing tip for camber shaping. In the same year, Maxime Bayon De Noyer[41] used an actuator called the OPSA (see Figure 2). The control moments are achieved by placing the piezoceramic stack, which uses the more efficient d_{31} coefficient, parallel to the controlled structure at a distance from the neutral axis and at a selected orientation. The actuator assembly is made of two structural elements bonded to the controlled system. The active element, a piezoceramic stack, is clamped with rounded contacts between the blocks for reliability issues. Also in 1999, Spangler and Jacques[47] were able to test the buffet load alleviation (BLA) on a full size F/A-18. The testing in this effort was primarily ground tests. This was the first time piezoelectric actuators were used for control on a full size aircraft. Fifty percent reduction in RMS was achieved but only at very benign conditions. However, they found that linear amplifiers were not capable of the performance to achieve 50 percent reduction in the most severe buffet conditions. This research also first indicated the limitation of piezoceramic wafers, which use the d_{33} coefficient.

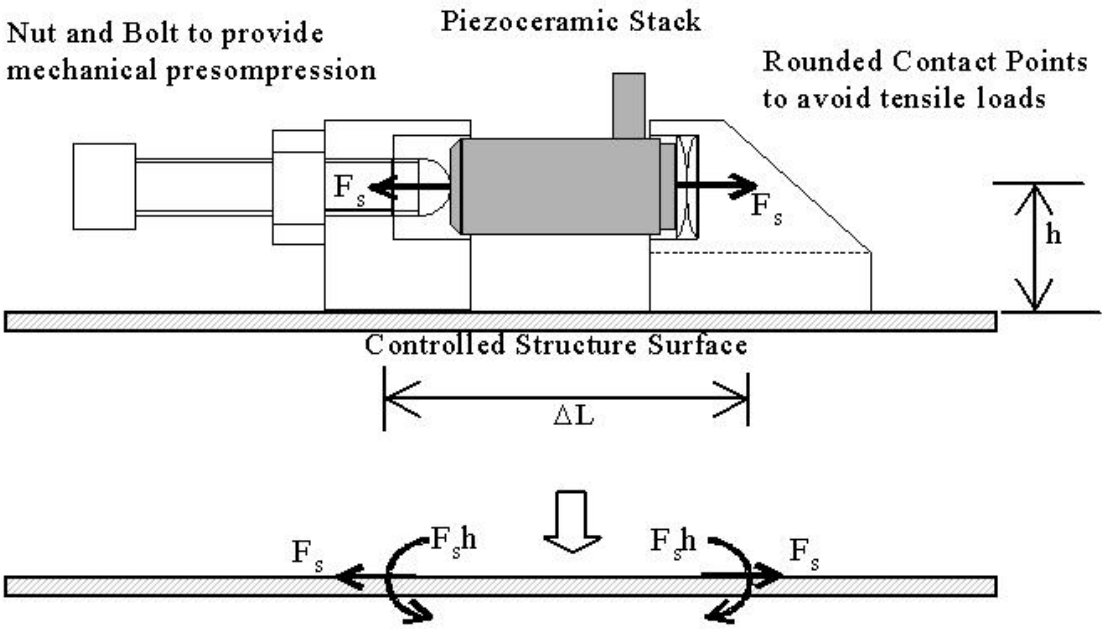

Figure 2: OPSA

In 2000, Kandil[52] used computer models to investigate the effectiveness of adaptive flow control for twin-tall buffet alleviation. This method used control ports at locations on the vertical tail surface. The idea is to use positive or negative flow control to reduce the pressure differential across the tail surface thus reducing the vibration of the tail. In 2001, Flynn[58] showed that a permeable surface, passing air through a plenum, reduces the amplitude of the buffet excitation.

In 2001, Sheta[63] used additional blowing techniques, such as tangential central blowing (TCB), tangential vortex blowing (TVB), and tangential spanwise blowing (TSB) to inject high-momentum fluid into the vertical flow of generic fighter aircraft flying at 30° AOA. These techniques strengthen the vortex which delays breakdown of the flow. In the same year, El-Badawy and Neyfeh[56,57] used a saturation-based control and piezoceramic patches mounted near the root of the tail as vibration absorbers to reduce steady state vertical tail vibrations on a $1/16^{th}$ scale model of an F-15. Both linear and nonlinear vibration absorbers were tested. Sensing was in the form of strain gages. In weakly nonlinear systems, internal resonances may occur if the linear natural frequencies are commensurate and these resonances provide a path for energy exchange between modes. Saturation occurs if two natural frequencies with quadratic nonlinearities are in a 2:1 ratio. When the higher mode is excited with enough energy that it saturates the overflow, energy is passed to the lower mode. Numerical nonlinear models were developed using the method of multiple scales. The frequency suppressed was at primary resonance. Experiments were conducted using MATLAB®/SIMULINK®, positive position feedback control, and a Dspace digital signal processor (DSP), which verified these results. In the same year, Burnham et al.[55] developed numerical models of an F/A-18 vertical tail which used active rudder and piezoelectric actuators in tandem.

The BLA system uses the most effective features of two systems; the rudder actuator and control surface are used to control the response of the tail first bending mode near 15 Hz, and piezoelectric actuators are used to control the response of the second tail mode, tip torsion, near 45 Hz. The overall performance of the BLA system produced 70 to 30 percent vertical tail buffet response reductions for flight conditions ranging from moderate to severe buffet. This was accomplished with a maximum commanded rudder position of 2° (15 Hz) and about 10 lb of piezoelectric actuators attached to the vertical tail skin and operating at a peak power level of 2000 watts. Also in 2001, Appa et al.[54] modeled a smart rudder system in which piezoelectric actuators were installed in the rudder at the hinge line. This system is called the Active Control Surface Modal (ACSM) device, and it generates unsteady aerodynamic damping to alleviate more effectively the aeroelastic structural instability, vibration, and dynamic loads. An ACSM deformation is created by means of pairs of activated actuators. The lightweight upper and lower surface skins were activated at high frequencies that encompass the wide band spectrum of buffet, gust, and self-excited flutter phenomena. Although the ACSM was an integral part of the rudder, independent control laws could be employed to serve the buffet load and the flight control requirements. Thus, the ACSM device generated unsteady aerodynamic damping in out-of-phase with the external (buffet/gust) or self-excited air loads (flutter) to reduce or eliminate the undesirable dynamic effects on the aircraft. Results showed 60 to 80 percent reduction in peak stress.

In 2003, Hanagud et al.[42,64,69] developed a method to determine the exact number of OPSA actuators, their location and actuation, and to attain the needed control authority to control tail vibrations based on the geometry of the actuator, the piezostack used as the active element and the aerodynamic force on the tail. The closed loop theory was developed based on the use of acceleration feedback control (AFC) where the sensor is placed at a location for optimal

observability. One of the very important issues for the control designer is adding additional electronic damping to the controlled structure while avoiding any change in its natural frequencies and avoiding the creation of new frequency peaks in the closed loop response. In the root locus plot, a particular point of interest is a single degree of freedom system controlled by acceleration feedback control, as shown on Figure 3. Where the point and the plot lines cross (as indicated with the o symbol) is called the crossover point. At this point, the closed loop poles of the structure and of the compensator coincide. This means that the frequency response of the closed loop system will only exhibit a single peak. In Hanagud's work, crossover point theory was used as the control design parameter for a system with a single degree of freedom. This was modified to control a multidegree of freedom system. Bending, torsion, and coupled modes can be controlled with this methodology.

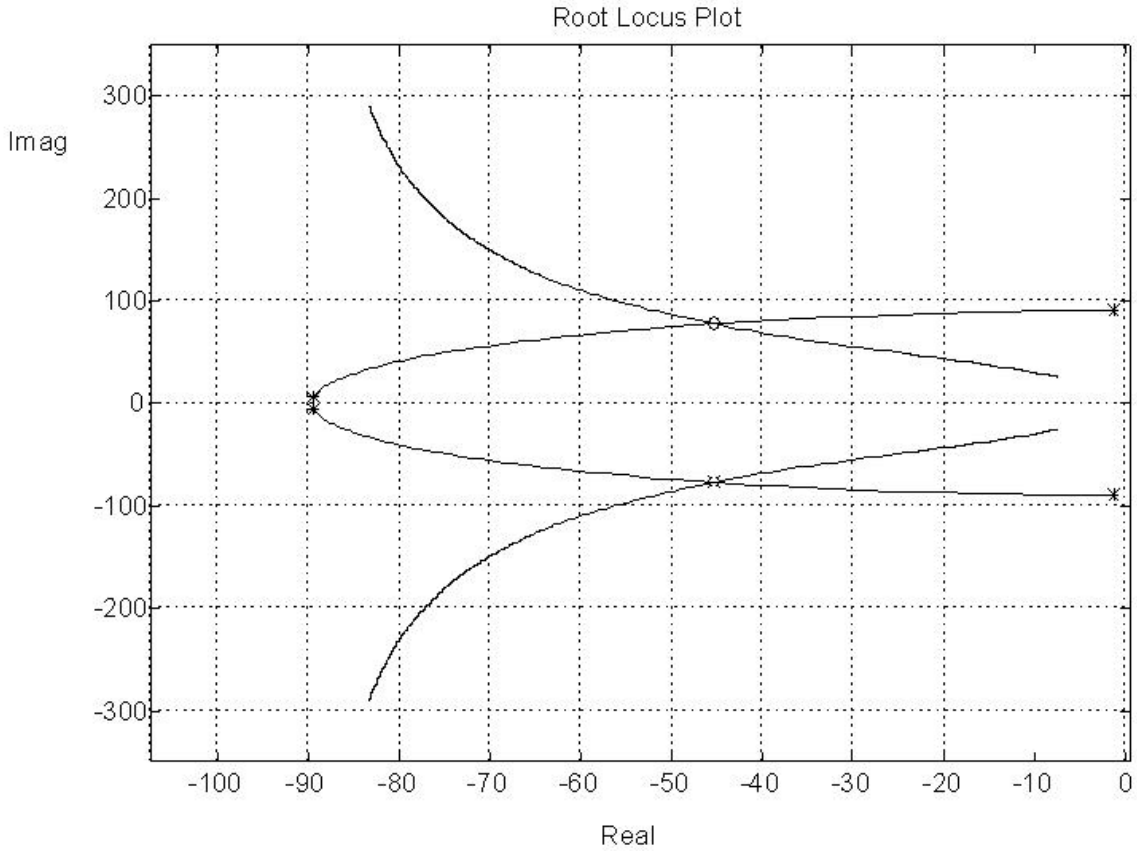

Figure 3: Single Degree of Freedom System under Acceleration Feedback Control Root Locus Plot and Cross Over Point (o)[51]

Sheta[72] numerically investigated piezoceramic lead zirconate titanate (PZT) actuators installed on the inboard and outboard surfaces of the vertical tail of an F/A-18 to control the buffet responses in the first bending and torsion modes. A SISO controller is designed to drive the active piezoelectric actuators. A multidisciplinary analysis was performed using taking into account the fluid dynamics, structure dynamics, electrodynamics of the piezoelectric actuators, fluid-structure interfacing, and grid motion, which are integrated into a multidisciplinary computing environment that controls the temporal synchronization of the analysis. Results show peak values of the PSD of tail tip acceleration are reduced by as much as 22 percent in the first

bending mode and by as much as 82 percent in the first torsion mode. RMS values of tip acceleration are reduced by as much as 12 percent.

In 2004, Ferman[73] performed subsonic wind tunnel tests of a 4.7 percent scale model of the F-15 fighter. Tangential blowing was introduced from three points: the nose, the wing-root leading edge, and the gun bump, blowing back to the tails in a Coanda-like effect. Several blowing pressure values were used at AOA from 0 to 32°. Results showed that blowing was seen to lower the buffet pressures on the tails and to reduce the structural response. The level of response varied somewhat between bending and torsion moments and acceleration data. Also, the trends depended upon AOA, yaw, and frequency bands. In some cases, blowing actually increased the response slightly. The most effective blowing position was the wing blowing position, followed by the gun position, and then the nose position, which was the least effective.

2.2 Neural Networks in Active Damping of Structures

Over 50 years ago, neural networks were developed from an idea that any logical problem can be solved by a suitable network composed of binary decision nodes[25]. A single node or neuron is shown in Figure 4. The following describes how this single neuron works:

1. The scalar input x is transmitted through a connection where it is multiplied by a scalar weight *w* to form the product *xw*.
2. The transfer function *F* uses the input *xw* as the argument and outputs the scalar *y*.
3. By using some yet to be known criteria we could adjust the weight *w* to an optimal value and, therefore, fine tune *y*.

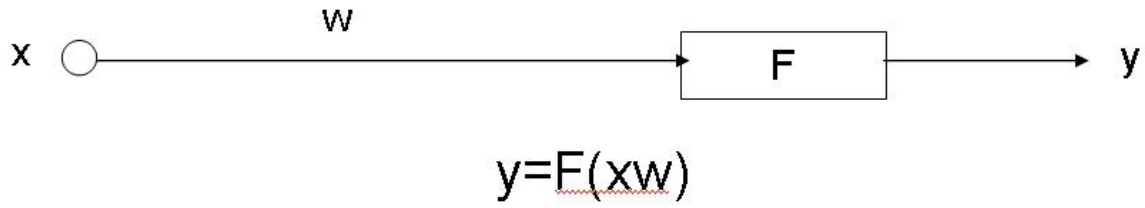

Figure 4: An Artificial Neuron

Typically, one neuron is not enough to respond just like a desired function because there may be more than one input or the problem may be more complex than a single neuron can handle. Therefore, we can use many neurons in a network, as seen in Figure 5. The real power of a neural network comes from the ability to adjust the weights between the nodes. The process of adjusting these weights is called training the network. This training typically proceeds as follows:

1. An example with a known output is fed into the inputs of the network.
2. The calculated network output is compared to the expected output and any difference is considered error.
3. The magnitude and sign of the error is used to adjust the network weights.

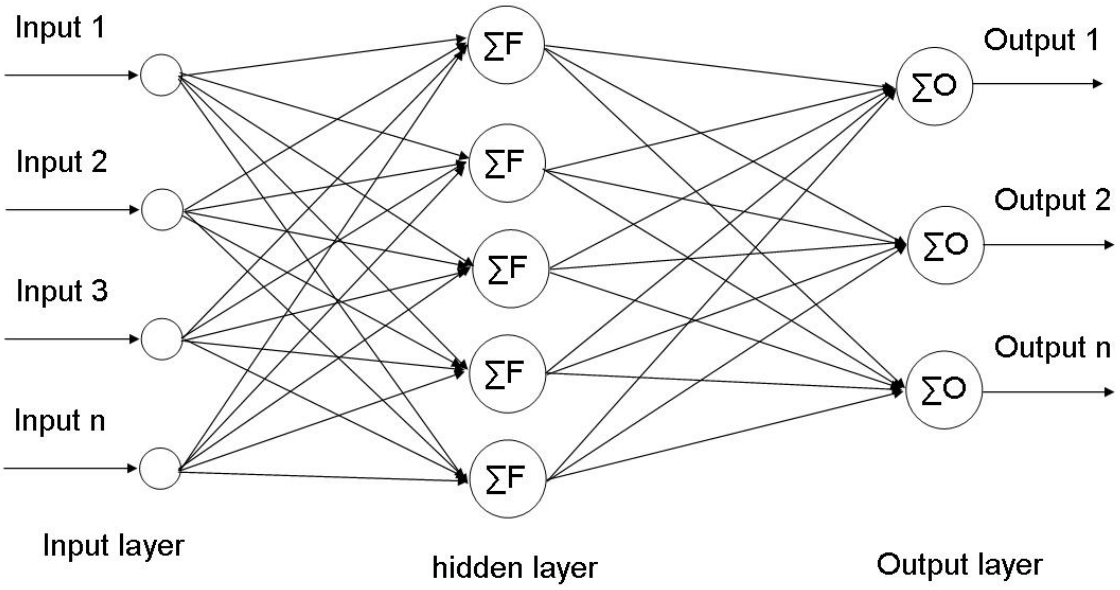

Figure 5: A Typical Neural Network

This process repeats until the magnitude of the error falls within a specified tolerance. The process of taking this error and adjusting the network weights is called back propagation. Because these networks are so powerful, they have been used in a wide variety of complex applications such as earthquake detection and characterization, pattern recognition, modeling of dynamic systems, statistical trends, and even control. Neural networks are used for control when the plant of the system is either nonlinear or there are uncertainties that a robust linear controller cannot control. There have been many efforts to use neural networks to control vibrations in structures. In 1992, Nikzad and Ghaboussi[5] used what is called a multilayered feed forward networks (MFNs), with a delta bar delta back propagation learning rule, and applied it to vibration control of mechanical systems. The neural network was able to reduce vibration more efficiently than the conventional controller due to the ability of a neural network to produce a better sampling period phase delay compensation and a reduction and filtering of the higher frequency noise. In conventional implementation of digital control, noise can result in a phenomenon referred to as controller spillover.

In 1993, Drakunov et al.[8] used a neural network along with a sliding mode controller to control a numerical model of an Euler-Bernoulli beam with piezoelectric strips along one of its sides. The neural network is used to learn and perform integral transformations of the distributed parameter system. This can be very difficult to do analytically, however, and forces the transformed system to behave as a second-order system.

In 1995, Long et al.[18] developed simulation models of neural network controllers for vibration suppression using sensors and actuators that were noncollocated. Actuators and sensors may be noncollocated for a variety of reasons. Optimum control location can be different from the point of control observability. Damage to the structure and other physical constraints may not allow collocated sensor/actuators. Long controlled a cantilever beam using a forward dynamics controller. The control procedure works as follows: the state at time k is fed to the neurocontroller, which generates a list of trial controls spanning the range of admissible control.

These controls together with the state (at time k) are fed to the forward dynamics neural net. A trial response for each trial control is produced and the corresponding cost (J) is computed.

The control corresponding to the smallest J is selected, which produces a new plant response at time k+1. For each time step, this procedure is repeated. During an on-line learning interval, the plant output is compared to the estimated plant output from the forward dynamics neural net model. The error is used in back propagation to update weights of the neural network. The excitation that was used was impulse, single sine wave (1 Hz) and composite sine wave of seven different frequencies. They were able to obtain an order of magnitude or more reduction of beam tip displacement.

In predictive control the plant model is used to predict future behavior of the plant, which then can be used for future control performance[76]. In 1996, Pado and Damle[26] used a cantilevered beam and a neural network with predictive control to run at much higher band widths. The plant consisted of a 28-inch aluminum beam with an accelerometer at the free end and a PZT actuator close to the root. The first two modes of the beam are at 5 and 31 Hz. A 60-MHz Pentium-based PC was used to run the test, and a digital controller was used at 185 Hz. Neural networks have advantages over conventional control schemes from the fact that they can be simpler, more cost effective, and can learn in a time varying manner due to parameter changes. For this neural predictive control, the neural network is shown in Figure 6.

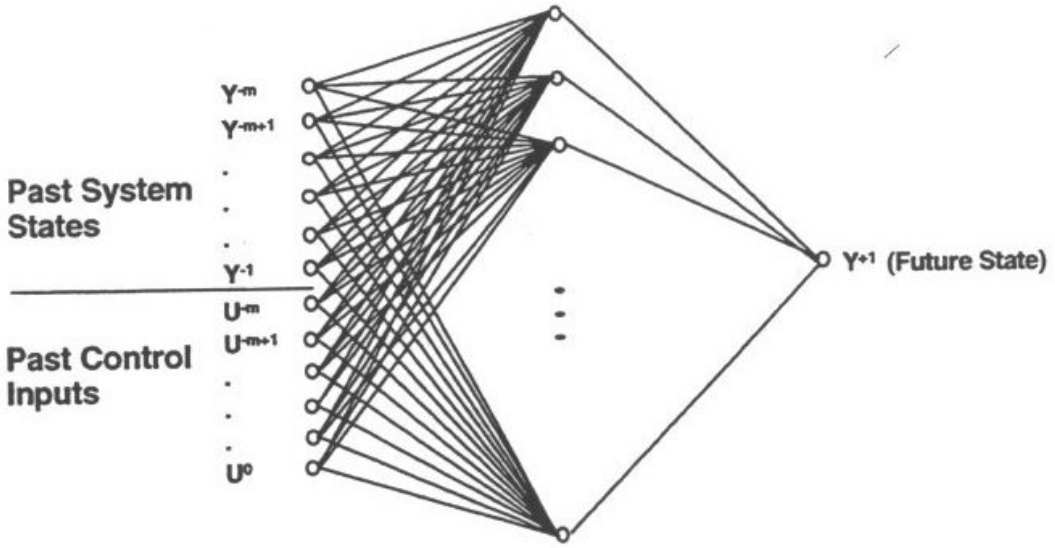

Figure 6: A Neural Network Plant Model for Predictive Control[26]

The neural network used in this effort is called the multilayer Perceptron (MLP) and is the active element in the neural predictive control (NPC). It uses back propagation to train the network. This type of network is called a universal approximator which is able to learn any function to any degree of accuracy, is very compact, and provides excellent generalization. It is also able to model nonlinear systems. The drawback of this type of neural network is that it takes longer to train than other types of neural networks. To begin the experiment, the network must be trained. They drove the beam with a random excitation from 0 to 185 Hz. The response was fed into the neural network and passed through a digital tapped-delay-line for *m* past time steps. Both the current and past control inputs are also fed into the network in the same manner. As in typical back propagation the output from the neural network is compared actual sensor output and the difference between the two are used to adjust the weights of the neural network. Once the

network is trained, the current state information is fed into the neural network as well as the first proposed control input. Referring to Figure 7, the multistep horizon look ahead takes this input and projects n steps into the future.

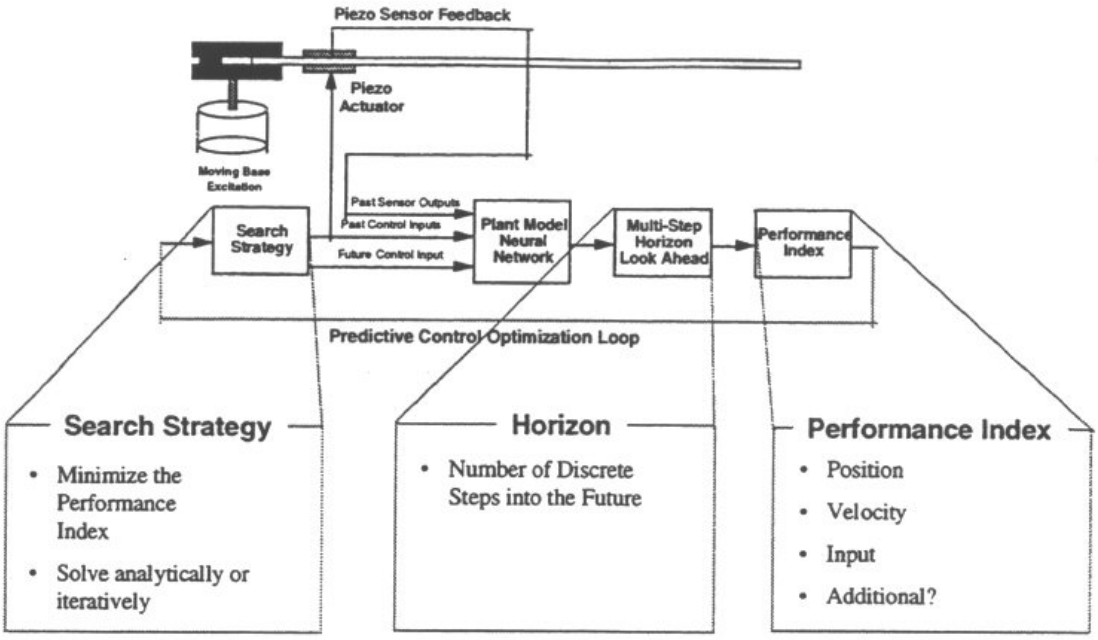

Figure 7: Predictive Neural Network Implementation on a Cantilevered Beam

The value of n is determined by the modes of the plant and the control rate. The value of n is between 1 and 20 and is called the horizon. This horizon is then passed to the performance index which is a cost function. It is comprised of future predictions of the neural network model (position), model derivatives (velocity), and the proposed control (input). Each of these parameters can be weighted and tailored to a particular system using the following equation:

$$C = \sum_{i=1}^{n} \left(G_P Y_i^2 + G_v \dot{Y}_i^2 + G_I I^2 \right) W^i \quad , \tag{1}$$

where

C is the cost of the selected input (I)
i is the horizon index
n is the horizon window
G_p is the position gain
Y_i is the predicted state of the plant at horizon i
G_v is the velocity gain
G_I is the input gain
W_i is the future state weighting factor.

G_p and G_v are the most important parameters to adjust to obtain the desired result of the controller. If $G_I = 0$ this can cause the system to go unstable. Once the value of C is determined, it is passed to the search strategy. If the system to be controlled is linear, the searching can be rather quick. However, if the system is nonlinear and no assumptions are used about the

nonlinearities, then the search time can be extremely long. This is the biggest drawback of this control scheme. In test results, it did provide better vibration suppression than proportional integral derivative (PID) and pole-zero controlled response.

In that same year, Lu et al.[23] used a neural network to control vibrations on a model of a simply supported beam with structural nonlinearities, modeling error, parameter imprecise, and disturbance. Some of these conditions are also called uncertainties. Specifically, they developed a neural algorithm to design the structural vibration control system and a neural network controller. The control has a two-step process: 1) learn the dynamic characteristics of the structure, and 2) then control the system to obtain results as good as an linear quadradic regulator (LQR) control system. Results show that this controller could reduce the vibrations within 7 seconds.

Also in 1996, Wang and Sinha[29] addressed the issue of controlling uncertainties in a single degree of freedom system by the development of a hybrid controller. In a numerical model, this hybrid controller is composed of a classical discrete-time LQR and two feed forward multilayer neural networks known as MNNA and MNNB. The neural networks control the uncertainties in the system. The uncertainties are in the form of system parameters such as stiffness and damping and excitation frequencies. MNNA compensates for modeling errors in the output of the model. MNNB corrects the control input for the vibration response. To test this controller, a spring-mass system was subjected to a sinusoidal excitation. Different values of stiffness and damping were introduced into the model with very good reduction in the amplitude of the vibration for steady state vibrations. Both neural networks were trained prior to testing. In 1998, Spencer et al.[39] used an adaptive neural network to control vibrations on a cantilever beam. The actuators are piezoceramic based and apply control moments at specific points along the beam. The excitation forces were in the form of periodic external disturbances. This was modeled numerically and tested experimentally. In the numerical model, the beam could rotate at each point that a actuator was placed. The actuators were modeled with torsional springs, and the external disturbances were torques applied at these joints. The uncertainties in this system are 1) the loading which may be unknown except that it is continuous and periodic, 2) changes in the system mass, and 3) changes in the system stiffness. Adaptive techniques that require an explicit, parametric description of the uncertainty cannot be used. The new technique used to solve this uses a class of universal parameterizations drawn from approximation theory. This acts as a curve fitting mechanism providing a real-time estimate of the external forces. The controller has three parts: 1) an underlying proportional-derivative component, 2) an adaptive component, and 3) a neural network. The reduction in vibration amplitude was more than an order of magnitude.

In 2001, Jha and He[60] developed an adaptive controller called the direct adaptive neural network controller (DANNC) to reduce vibrations in an experimental cantilever beam. An adaptive neural network (ANN) learns while it controls so there is no pre-training. This type of neural network is required for applications where changes in the system or environment, including uncertainties, will occur and the controller must adapt to these while controlling the plant. Real-time training used the Levernberg-Marquardt back propagation algorithm. Bonded piezoelectric PZT actuators were used and acceleration was measured at the free end of the beam. The goal of the controller was to control the first mode subjected to impulse, and band-limited white noise disturbances. The first two modes of the beam occurred at 6.2 Hz and 37 Hz. For the first mode impulse excitation, the settling time was reduced over 80 percent. For the sine wave, the controller learning was completed in four cycles (about 0.5 second) and RMS of the vibration amplitude was reduced by 90 percent. However, during training, the closed loop

response is somewhat larger than the open loop. Even though the goal was to control the first mode, the controller was changed to control the second mode. The RMS for this mode was reduced by 86 percent. During a white noise disturbance (0 to 50 Hz), the RMS was reduced by about 50 percent. Sharma and Calise[62] derived a method to augment existing linear controllers with an ANN. The benefit of augmenting with a neural network is that you preserve the current controller architecture. This just adds the neural network signal to the linear controller signal. This can be applied to both SISO and MIMO control. Augmenting a neural network broadens the applicability of the controller. This network was numerically modeled and showed a small 2.5 percent error in position tracking. The authors stated that this error could be further reduced by adjusting the neural network learning rates. Some of the restrictions of this controller are that it requires full state feedback and it attempts to match the closed loop plant to the response model state for state. Any uncertainties must satisfy the matching condition in which the neural network tries to enforce the same relationships between the plant states and their derivatives as those in the response model. In 2003, Bong-Jun[67,68] et al. experimentally validated this work by successfully controlling a three-disk pendulum and an inverted pendulum using this ANN.

2.3 Neural Networks in Aeroelasticity

One of the first uses of neural networks in aeroelasticity was to characterize the buffet pressures on the aircraft structure. These buffet pressures come from a highly nonlinear relationship between upstream geometric and aerodynamic parameters. In 1993, Pado and Jacobs[9] needed to predict the location, magnitude, and frequency content under any flight condition from these buffet pressures. Even though there have been many important advances in the field of computational fluid dynamics, they are not capable of predicting the separated flow dynamic pressure environment around the vertical tail. Wind tunnel tests could be conducted, but this can be very expensive and can occur too late in the design process to allow for major structural changes. This could only be accomplished with a neural network. However, neural networks could only focus on overall parameters such as error, so a new neural network had to be developed. They developed a new hybrid cascading neural network (HCNN) which has the ability to both extrapolate and perform the dynamic scaling necessary to retain shape features of the pressure frequency spectra. This was accomplished while using noisy data. To train this, HCNN data was acquired from NASA Langley Research Center from their work in vortex-tail interactions. Pado and Jacobs used a rigid tail of a 76± delta wing model with five pressure sensors on the vertical tail. This tail was adjustable along the longitudinal axis. Many neural network architectures were considered, such as radial basis function network, general regression neural network, and multilayer Perceptron trained with back propagation. Only the radial basis function network coupled with multiquadratic function could accomplish the distance interpolation, leading to the required extrapolation and, thus, the hybrid label. Stresses were modeled using a FEM as the aerodynamic pressure is greatest at the leading edge of the tail and deceases toward the trailing edge. For frequency-dependent data, a 49-output architecture was used to construct the PSD in the frequency range of interest. A single neural network cannot handle the variation in PSD as a function of AOA, especially at low and high magnitudes, so a scaling or cascading method was derived. The predicted RMS pressure is input to the multilayer perception, which is used to predict the basic shape of the PSD. This performs a dynamic scaling in which the RMS pressure is used to scale and then later unscale the PSD. Finally, the RMS signal and the modulating signal are used to construct the unscaled PSD. Results were very good except for low AOA where overpredictiveness of RMS pressure occurs. In 1994, Jacobs et

al.[14] extended the model to include a twin flexible tail. The two tails could be adjusted laterally so that the tails could be tested inside and outside the vortex flow. This allowed further HCNN training for future tail design efforts when considering tail buffet.

One of the early attempts at active control of an aeroelastic structure was in 1995[53] in a joint NASA/Boeing effort, as part of the Adaptive Neural Control of Aeroelastic Response (ANCAR) project, using transonic wind tunnel data to train a neural network for flutter suppression. The goal of this program was to develop a neural network-based adaptive control scheme using what is called the benchmark active controls technology (BACT) wind tunnel model. The BACT wind tunnel model is a rectangular wing with a NACA 0012 airfoil cross section. Trailing edge control surfaces and spoilers can be independently controlled. The neural network was used to schedule 56 flutter suppression control laws with fixed gain. Each law used a corresponding state space model. The state space models in this design used the same structural and aerodynamic models with varying Mach number and dynamic pressure. The range of Mach numbers was 0.3 to 0.9 and the range of dynamic pressure was 75 to 250 psf. These state space models were used to design a fixed gain control law which was optimized to minimize accelerometer output for each combination of Mach number and dynamic pressure. To stabilize and minimize the response over all the state space models a fixed gain feedback control law was designed. To eliminate any drift due to bias in the sensors and washout filter was used. Root locus and zero placement were used in the design of the feedback control law as follows:

$$\frac{s(s^2+12s+520)}{s^4+27s^3+491s^3+4515s+13050}\ . \qquad (2)$$

For the neural network, Equation (2) was tailored to each of the 56 state space models. The order of the numerator and denominator was the same as Equation (2) and took the form of the following:

$$k\frac{s^3+a_2s^2+a_1s}{s^4+b_3s^3+b_2s^2+b_1s+b_0}\ . \qquad (3)$$

The neural network was trained using back propagation. The examples used to train the neural network were in the continuous domain rather than the discrete domain because the continuous domain coefficients vary smoothly as a function of Mach number and dynamic pressure and do not require high numerical precision. Experimental results clearly show that trailing edge acceleration RMS is lower with the neural network than the fixed gain controller by approximately 10 percent.

In 1996, Lichtenwainer et al.[21][22] used NPC, as part of the ANCAR program, to control flutter on NASA's BACT wing model in the Transonic Dynamics Tunnel (TDT) at NASA Langley Research Center. On the wing, the trailing edge flap, as is shown in Figure 8, was used as the actuator, and an accelerometer next to the flap was used as the sensor. The NPC was used in a SISO control scheme whose control laws are a function of Mach number and dynamic pressure. Phase I of this work used both a fixed gain controller and a model predictive control (MPC) neural network for semi-adaptive control to tailor poles and zeros at each M and q. More specifically, a set of 56 combinations of Mach (M) and dynamic pressure (q) were created and used to train the network. Results showed that the neural network reduced the RMS slightly more

than the fixed gain. Phase II implements a fully adaptive flutter suppression system using the MPC architecture in Figure 9.

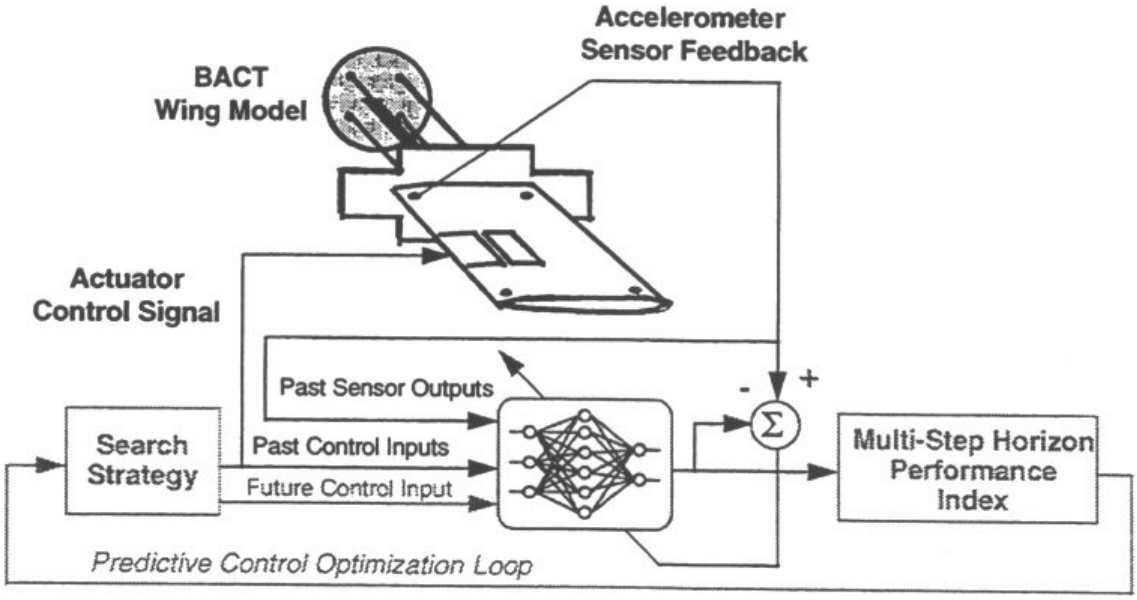

Figure 8: NPC System Architecture on BACT Wing

They state that this phase II neural network can be trained before use and updated on-line to cope with changing flight conditions and plant dynamics. In these tests, the SISO control was demonstrated up to 500 Hz. The control works as follows: Starting with an untrained network, white noise is sent to the aileron for 4 seconds, and then there is a 2.7-second learning interval, followed by a 6.7-second control interval. After this, updates are allowed every 6.7 seconds; however, this can change depending on the CPU speed, control cycle rate, and the amount of data required for accurate plant modeling. This type of control shows an improvement over the semi-adaptive controller. However, the search and learning times can still take some time depending on the complexity of the control scheme and the plant model. Once this MPC had been shown to be somewhat effective in flutter suppression, the next logical application was tail buffet alleviation. In 1998 and 1999, Pado and Lichtenwalner[38,46] were the first to use a neural network to actively control tail buffet. This research comes from a joint Boeing, St. Louis/NASA Langley Research Center effort to reduce the tail buffet effect that reduces the fatigue life of many aircraft. Neural networks were chosen as the solution due to their ability to model the plants nonlinearities and their adaptability. An MPC neural network was created as seen in Figure 9. A wind tunnel test was again setup at NASA Langley's TDT using a $1/16^{th}$ scale model aircraft of a YF-17 (later known as the F/A-18). The model was configured with a scaled flexible vertical tail, mounted on the left side of the model. The control mechanism on the starboard tail is an active rudder to control the first mode (bending) and a PZT patch to control the second mode (torsion). The port tail had two PZT patches as actuators to control bending and to control torsional vibrations. The flexible tails use an aluminum spar and balsa wood cross sections. A hydraulic actuator is incorporated into the tail to move the rudder during the controlled runs. The strain gages are used as sensors to control bending and accelerometers were used as sensors to control torsion.

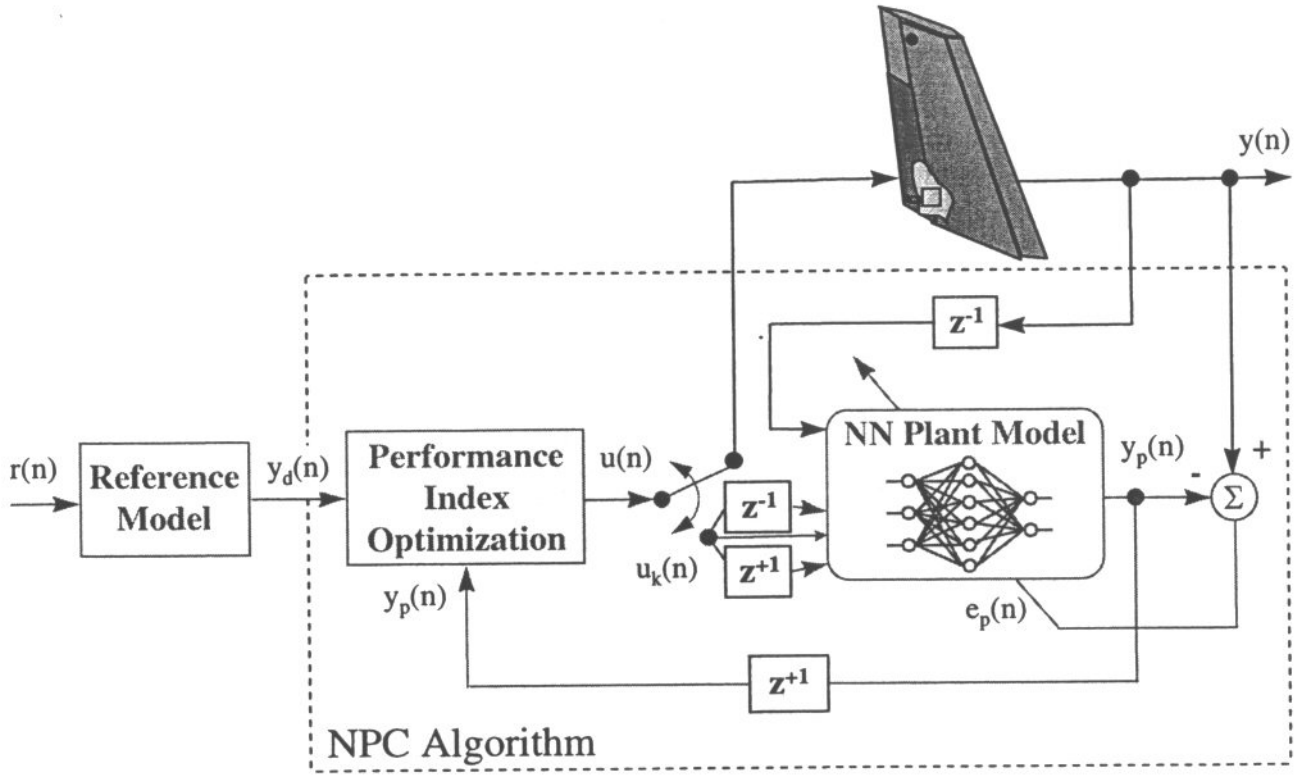

Figure 9: NPC System Architecture on BACT Wing Phase II

Due to the fact that the magnitude of buffet is a function of dynamic pressure and AOA, RMS pressure was experimentally determined at six different AOA between 20 and 40° and at dynamic pressures of 3.5, 5.2, 7.8, and 10.0 psf. When these AOA and pressures are scaled up to correspond to the full size tail, they cover the range in which 80 percent of tail buffet damage occurs. They state that over 80 percent of the tail damage occurs in these regimes. There were two modes of interest in the test; first, bending at 18 Hz and first torsion at 58 Hz. Control authority is a measure of how effective the control is for targeted control states. In this case control authority was measured by using a rotational variable displacement transducer (RVDT). This was curtailed starting at 35 Hz, which decreased the torsion mode control authority by a factor of 4. To overcome this, the PZT patches were used to control torsion. For coupled modes, both the rudder and PZT patch were used to reduce RMS, which involved scaling the system up from SISO to MIMO. The tests planned to control the first bending mode, and then the first torsional mode. They were not able to control both modes simultaneously due to time limitations in the wind tunnel. The neural network was trained using the response during each condition, Mach number, dynamic pressure, AOA, and pitch rate. One of the key components of this neural network is a second neural network used to model the plant to control nonlinear behavior. Because the rudder opposes aerodynamic forces, the plant model had to be created under very noisy conditions, which led to a signal-to-noise ratio (SNR) of 1-to-10. For training purposes prior to implementation they created the neural network plant model mentioned above using rudder to strain gage transfer functions. They started with 7° AOA and performed random excitation tests from 0 to 200 Hz. The output from the network is compared to the actual sensor output and the weights of the neural network plant model are adjusted using back propagation. The SISO system is trained using the same method as mentioned with the BACT wing except

that for the MIMO system, they tried two different techniques. The first technique used a single integrated network. Past actuator control inputs from each of the actuators and past states from the sensors are fed in to a single neural network. Both horizons are used in the cost function along with network weights. This then is used in the search strategy, which must now search in a two-dimensional (2-D) space (this also uses twice the number of parameters). This technique can be so long, that it is unwieldy. This is due to the 2-D space in the search strategy adding an additional dimension and more complexity. The second technique used multiple, independent SISO controllers. These are separately trained but used simultaneously.

For the SISO controller, first bending reduction in RMS was 16 percent. First torsion reduction was 12 percent. However, when both controllers were run concurrently, first bending RMS reduction went from 16 percent to 15 percent. First torsion RMS reduction went from 12 percent reduction to 6 percent. The MIMO solution had somewhat better results. First bending was reduced by 30 percent and 10 percent in first torsion. The starboard tail had less reduction in RMS. This shows that using a control surface for tail buffet alleviation is not as effective as a separate actuator used separately for this purpose.

3.0 Controller Design

We will first design the linear acceleration feedback controllers that will control bending and torsion modes of interest. It is assumed that one sensor (e.g., accelerometer), located at (x_a, y_a) on the vertical tail to be controlled, provides the input (i.e., the structural response of the tail) to controllers. The output of controllers are multiplied by gains γ_i and are applied to the actuators in OPSAs. Two sets of OPSAs are mounted on the tail structure. Each set of OPSA may include several PZT stacks, whose outputs are additive. As shown in Figure 10, the i^{th} OPSA is oriented at an angle α_i to the elastic axis of the tail.

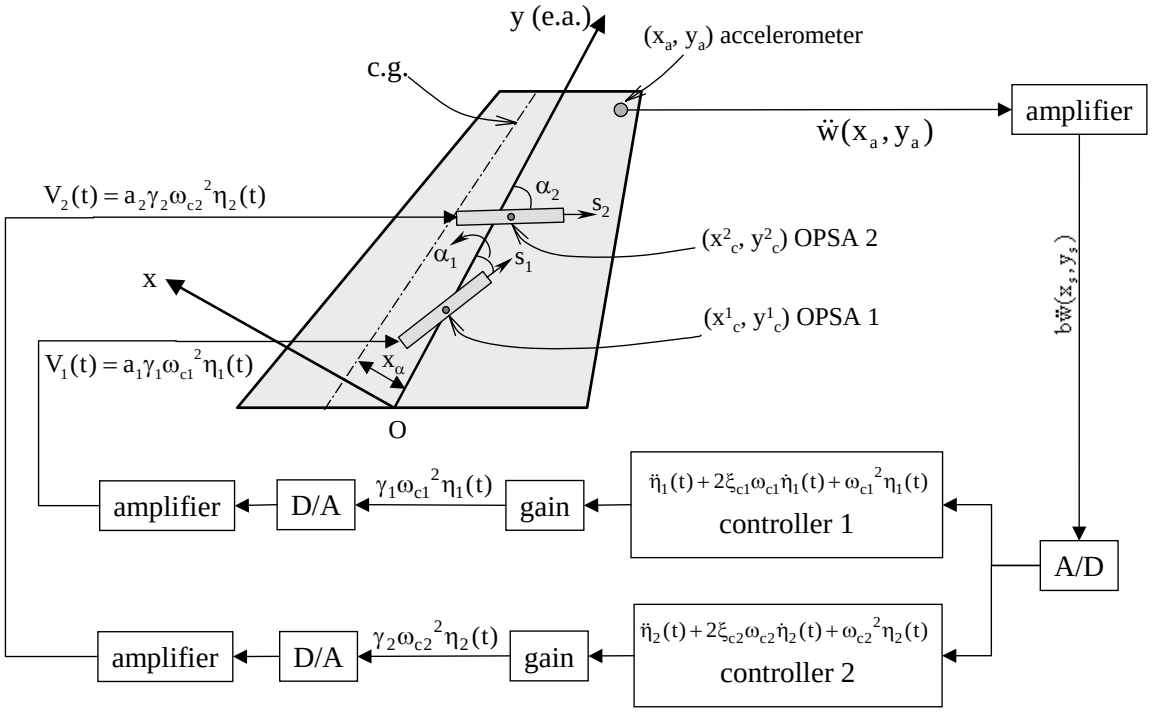

Figure 10: Diagram of the F/A-18 Active Linear Control System

The center of OPSA *i* is located at (x^i_c, y^i_c). When subjected to an electric field, the forces exerted by each PZT stack on the tail can be divided into two parts: two point moments (that can be decomposed into bending and torsion moments) and a pair of extensional forces. The governing equations for this closed-loop system are given by the following equation:

$$\begin{cases} m(y)\dfrac{\partial^2 w}{\partial t^2} - mx_\alpha(y)\dfrac{\partial^2\theta}{\partial t^2} + \dfrac{\partial^2}{\partial y^2}\left(EI(y)\dfrac{\partial^2 w}{\partial y^2}\right) = -\sum_{i=1}^{n} n_s^i F_s^i h\cos\alpha_i \dfrac{d}{dy}\left[\delta\left(y-y_2^i\right)-\delta\left(y-y_1^i\right)\right] + f_1(y,t) \\ -I_\alpha(y)\dfrac{\partial^2\theta}{\partial t^2} + mx_\alpha(y)\dfrac{\partial^2 w}{\partial t^2} + \dfrac{\partial}{\partial y}\left(GJ(y)\dfrac{\partial\theta}{\partial y}\right) = \sum_{i=1}^{n} n_s^i F_s^i h\sin\alpha_i\left[\delta\left(y-y_2^i\right)-\delta\left(y-y_1^i\right)\right] + f_2(y,t) \\ \ddot{\eta}_i(t) + 2\xi_{ci}\omega_{ci}\dot{\eta}_1(t) + \omega_{ci}^2\eta_i(t) = b\ddot{\bar{w}}(x_a, y_a, t) \qquad i = 1,\ 2,\ ...,\ n \end{cases}$$

(4 a, b, c),

where $f_1(y,t) = \int_c \Delta p(x,y,t)dx$; $f_2(y,t) = \int_c x\Delta p(x,y,t)dx$. (5)

$\delta(\cdot)$ is the Dirac Delta function. Generalized aerodynamic bending loads $f_1(y,t)$ and aerodynamic torsion loads $f_2(y,t)$ are given by Equation (5). It is assumed that the primary control force from the OPSA are by induced moments. The displacement of the tail at any position (x, y) of the tail, $\overline{w}(x,y,t)$, is contributed from both bending and torsional motions, as shown in Equation (6):

$$\overline{w}(x,y,t) = w(y,t) + x\,\theta(y,t) \quad . \tag{6}$$

The input voltage of OPSA $V_i(t)$ is the product of the actuator flexibility influence parameter a_i, controller gain γ_i and control signal $\omega_{ci}^{\,2}\,\eta_i(t)$. That is,

$$V_i(t) = a_i\,\gamma_i\,\omega_{ci}^{\,2}\,\eta_i(t) \qquad i = 1, 2, \ldots, n \quad . \tag{7}$$

In Equations (6) and (7), we introduce a sensor flexibility influence parameter *b* as well as actuator flexibility influence parameter a_i, by using Maxwell's reciprocal theorem. These coefficients take into account the effects of phases and geometries of the actuators and the sensor. Their values are taken from a numerically derived mass normalized first bending mode created in ABAQUS® 5.8 using a three-dimensional (3-D) cantilever beam.

We employ the mode summation method by including the first *N* important modes of the tail structure:

$$\overline{w}(x,y,t) = \sum_{j=1}^{N} g^j(x,y)\,q_j(t) \quad , \tag{8}$$

where $g^j(x,y)$ is the j^{th} coupled bending-torsion mode shape of the tail, we can write

$$\begin{aligned} w(y,t) &= \sum_{j=1}^{N} g_w^j(y)\,q_j(t) = \{\boldsymbol{\alpha}(y)\}^T[\boldsymbol{\Phi}]\{\mathbf{q}\}, \\ \theta(y,t) &= \sum_{j=1}^{N} g_\theta^j(y)\,q_j(t) = \{\boldsymbol{\beta}(y)\}^T[\boldsymbol{\Theta}]\{\mathbf{q}\}, \qquad \textit{where } \{\mathbf{q}\} = \{q_1,\ \cdots,\ q_N\}^T \end{aligned} \quad , \tag{9}$$

where $\{\alpha(y)\}$ and $\{\beta(y)\}$ are characteristic vectors of selected bending and torsion modes respectively. $[\Phi]$ and $[\Theta]$ are the eigen vectors listed as in Equation (9). The number *N* of the bending-torsional coupled modes should be less than $M = M_1 + M_2$, which are the numbers of considered bending and torsion modes. In these equations, q and η are the modal coordinates of the structure and of the compensator; respectively; ω_s, ω_c, ζ_s and ζ_c are the natural frequencies and the damping ratios of the structure and the compensator, respectively; and γ is the scalar gain applied to the feedback signal.

The first step of the procedure is to design the controller. This begins by first controlling the first bending mode by assessing the number of stack needed for control. For each mode that is to be controlled the closed-loop system reduces to a 2 degree of freedom AFC system (one for the structure and one for the controller) as follows.

$$\begin{cases} \ddot{q}_i + 2\xi_s\overline{\omega}_i\dot{q}_i + \overline{\omega}_i^{\,2}q_i = -n_s^1\overline{a}\,\gamma_1\omega_{c1}^{\,2}\eta_1 + \bar{f}_1(t) \\ \ddot{\eta}_i + 2\xi_{ci}\omega_{ci}\dot{\eta}_i + \omega_{ci}^{\,2}\eta_i = \bar{b}\,\ddot{q}_i \end{cases} , \tag{10}$$

where

$$\overline{\omega_i}^2 = \omega_i^2\left(1+\Omega^{-1}n_s^1 k_s^{\varepsilon} h\left(\cos\alpha_1\{\mathbf{\Phi}^1\}^T\{\mathbf{d}_w\}+\sin\alpha_1\{\mathbf{\Theta}^1\}^T\left(\{\mathbf{d}_{x\theta}\}+\{\mathbf{d}_\theta\}\right)\right)\hat{a}\right),$$

$$\overline{a} = \Omega^{-1}\omega_i^2 k_s^E a_1 \hat{a}$$

$$\bar{f}_1(t) = \Omega^{-1}\omega_i^2\ \hat{f}_1(t)$$

$$\overline{b} = b\{\boldsymbol{\alpha}(y_a)\}^T\{\mathbf{\Phi}^1\} + x_a\{\boldsymbol{\beta}(y_a)\}^T\{\mathbf{\Theta}^1\}$$

$$\hat{f}_1(t) = \int_0^L\int_c \Delta p(x,y,t)\left(\{\mathbf{\Phi}^1\}^T[A_{11}]\{\boldsymbol{\alpha}(y)\} + x\{\mathbf{\Theta}^1\}^T[A_{22}]\{\boldsymbol{\beta}(y)\}\right)dx\,dy, \qquad \text{(11a, b, c, d, e, f, g, h)}$$

$$\hat{a} = h\left(\cos\alpha_1\{\mathbf{\Phi}^1\}^T[A_{11}]\{\mathbf{d}_w\}+\sin\alpha_1\{\mathbf{\Theta}^1\}^T[A_{22}]\{\mathbf{d}_\theta\}\right),$$

$$\{\mathbf{d}_{x\theta}\} = \left\{ x\frac{d\beta_1}{dy}\Big|_{(x_1^i,y_1^i)}^{(x_2^i,y_2^i)},\ \cdots,\ x\frac{d\beta_{M2}}{dy}\Big|_{(x_1^i,y_1^i)}^{(x_2^i,y_2^i)} \right\}^T,$$

$$\Omega = \{\mathbf{\Phi}^1\}^T[\mathbf{A}_{11}]^2\{\mathbf{\Phi}^1\} + \{\mathbf{\Theta}^1\}^T[\mathbf{A}_{22}]^2\{\mathbf{\Theta}^1\}$$

From Equation (11a), the OPSA is represented by the second term. This shows that the OPSAs stiffen the tail structure as the values of the second term are always positive. This stiffening causes the closed-loop system to have a slightly higher natural frequency $\overline{\omega}_1$ than that of corresponding open-loop system ω_1. The difference between these frequencies increases with the offset *h*, the axial stiffness of stacks, the number of stacks and the deflection curvature at OPSA location. It also depends on the aligning orientation of OPSA, α_1.

3.1 Transfer Functions for Each Controlled Mode

We can obtain transfer functions for both the open-loop and closed-loop systems. The transfer function of the response and the excitation for the open-loop system is given by Equation (12) give the closed-loop transfer functions of the excitation and the response, the controller signal and the response, the controller signal and the excitation, respectively.

$$G_{qf}^{open}(s) = \frac{Q_i^{open}(s)}{\overline{F}_i(s)} = \frac{1}{(s^2+2\xi_i\overline{\omega}_i s+\overline{\omega}_i^2)}$$

$$G_{qf}^{closed}(s) = \frac{Q_i^{closed}(s)}{\overline{F}_i(s)} = \frac{(s^2+2\xi_{ci}\omega_{ci}s+\omega_{ci}^2)}{(s^2+2\xi_i\omega_i s+\omega_i^2)(s^2+2\xi_{ci}\omega_{ci}s+\omega_{ci}^2)+\gamma_i\omega_{ci}^2 n_s^1\overline{a}\,\overline{b}s^2} \qquad \text{(12a, b, c, d)}$$

$$G_{\eta q}^{closed}(s) = \frac{\mathrm{I}_1(s)}{Q_1^{closed}(s)} = \frac{\overline{b}s^2}{(s^2+2\xi_{c1}\omega_{c1}s+\omega_{c1}^2)}$$

$$\mathrm{G}_{\eta f}^{\mathrm{closed}}(\mathrm{s}) = \frac{\mathrm{I}_1(\mathrm{s})}{\overline{\mathrm{F}}_1(\mathrm{s})} = \frac{\overline{\mathrm{b}}\mathrm{s}^2}{(\mathrm{s}^2+2\xi_1\omega_1\mathrm{s}+\omega_1^2)(\mathrm{s}^2+2\xi_{c1}\omega_{c1}\mathrm{s}+\omega_{c1}^2)+\omega_{c1}^2\gamma_1\mathrm{n}_s^1\overline{\mathrm{a}}\,\overline{\mathrm{b}}\mathrm{s}^2}$$

The Laplace transform of each variable is represented by the corresponding capital letter.

3.2 The ANN

The ANN in this work is based on one developed by Bong-Jun[67] et al. The modeling is constructed in MATLAB® 6.5.1 and Simulink®. The harmonic load at the end of the beam is considered all disturbance as the controller is tracking y = 0.

The first assumption that is made is the linear system can be both observed and stabilized. With that the system, in normal form, is generally as follows:

$$\begin{aligned} \dot{z}_0 &= f\left(z_0, x_1, \cdots, x_r\right) \\ \dot{x}_1 &= x_2 \\ &\vdots \\ \dot{x}_r &= h_0\left(z_0, x_1, \cdots, x_r, u\right) \\ y &= x_1 \end{aligned}, \tag{13}$$

where
$z_0 \in R^{\text{n-r}}$: The states of the internal dynamics
$u \in R^1$: Control variable
$y \in R^1$: Measurement variable
f_0 and h_0 : Unknown continuous functions
r is the strong relative degree of the system. This means it is the same at every point in the system. Because this is a linear system, the strong relative degree is simply number of poles-number of zeros. As seen in Equation (12), this will give r = 2. The value of n does not need to be known. If we take

$\xi^T \overset{\Delta}{=} \left[x_1 \cdots x_r\right], \xi \in R^r$ ξ is known as the partial state. Partial states are key in Simulink® analysis

$c^T \overset{\Delta}{=} \left[1, 0 \cdots 0\right], c_m \in R^r$ where c is the system output matrix. (14)

In this development we will use a plant model or an observer to determine the error.

At this point we can start to account for any uncertainty in the system. Per references [67] and [68], system Equation (14) can be written as and include the general form of the uncertainties.

$$\begin{aligned} \dot{z}_1 &= F_0 z_1 + g_0 x_1 + \Delta_2\left(z_1, z_2, \xi\right) \\ \dot{x}_1 &= x_2 \\ &\vdots \\ \dot{x}_r &= h_0^T z_1 + a_1 x_1 + \ldots + a_r x_{lr} + b\left[u + \Delta_1\left(z_1, z_2, \xi, u\right)\right] \\ \dot{z}_2 &= f_2\left(z_1, z_2, \xi\right) \\ y &= x_1 \end{aligned}, \tag{15}$$

where

z_1 : The modeled part of the internal dynamics measured from the frequency response function of the linear model ($\dot{y}$).

z_2 : The unmodeled portion.

Δ_1 = Matched uncertainty

Δ_2 = Unmatched uncertainty

$\dot{z}_2$ is assumed to globally exponentially stable.

Now, if we design the controller that will track y = 0, we have

$$\begin{aligned} \dot{x}_c &= A_c x_c + b_c(y_c) \\ u_{lc} &= c_c^T x_c + d_c(y_c) \end{aligned} \quad , \tag{16}$$

where

$x_c \in R^n$

$$\dot{x} = Ax + Bu = Ax + Bu_c + Bu_{ad}\, y = Cx$$

$$\dot{x}_c = A_c x + B_c y = Ax + Bu_c + Bu_{ad}; u_c = C_c x_c$$

$$\begin{bmatrix} \dot{x} \\ \dot{x}_c \end{bmatrix} = \bar{A} x_l + \bar{b}_r y_c \quad , \tag{17}$$

The $\bar{A}$ is designed to be Hurwitz.

Now that the form of the system is known, we can look at the control signal with the addition of the ANN. We can let

$$\begin{aligned} u &= u_{lc} - u_{ad} \\ \bar{b} &= B_1 \end{aligned} \quad , \tag{18}$$

where u_{lc} is defined in Equation (16) and u_{ad} comes from the ANN. When we apply this to Equation (15), we get

$$\begin{aligned} \dot{x} &= \bar{A}x + \bar{b}_r y_c - bu_{ad} + \Delta \\ \dot{z}_2 &= f_2(z_1, z_2, \xi) \\ y &= \bar{c}_y x \end{aligned} \quad , \tag{19}$$

where

$$\begin{aligned} x^T &= \begin{bmatrix} \xi^T & z_1^T & x_e^T \end{bmatrix} \\ \Delta^T &= \begin{bmatrix} \Delta_1^T & \Delta_2^T & 0 \end{bmatrix} \end{aligned} .$$

The objective of the control design is to augment the linear controller (u_{lc}) with the adaptive signal (u_{ad}) so that Δ_1 is cancelled and the output y tracks the reference model output y_l (with bounded error).

3.3 Adaptive Output Feedback Augmentation (AOFA)

In this section we summarize the governing equations of the ANN. As mentioned before, the ANN needs the error y>0. The error vector is defined as

$$E^T \stackrel{\Delta}{=} \left[(\xi)^T \ (z_1)^T \ (x_c)^T \right] \ . \tag{20}$$

As we are not concerned with the unmatched uncertainty, the modified error dynamics formulation can be used as

$$\begin{aligned} \dot{E} &= \overline{A}E + \overline{B}(u_{ad} - \Delta_1) \\ z &= \overline{C}E \end{aligned} \ , \tag{21}$$

where *z* contains the signals for feedback.

$$z = \begin{bmatrix} y \\ x_c \end{bmatrix} \ . \tag{22}$$

Because $\overline{A}$ meets the Hurwitz criteria, there exists a Lypunov solution P = P^T > 0 such that for an arbitrary Q>0, the following is true:

$$\overline{A}^T P + P\overline{A} + Q = 0 \ . \tag{23}$$

For most applications Q can have values between 1 and 3. As you can see from this development Δ_1 is a function of u_{ad} through u. Calise and Bong used this to show that we can design u_{ad} via the ANN design to cancel Δ_1.

In this section, a single hidden layer neural network is used to approximate Δ_1 due to the assumption that we are using the neural network to control the uncertainties in the disturbance Like all other neural networks, the ANN works by adjusting the weights between the node connections so that it can approximate a function (Δ_1). We need all the states in Equation (21) to calculate the error used to determine the weights and this application has those.

The general form of the adaptive signal is as follow:

$$u_{ad} = u_{nn} = \hat{M}^T \sigma\left(\hat{N}^T \varphi\right) \ , \tag{24}$$

where
φ: Network input vector
σ : The sigmoid or squashing function of the nodes in the hidden layer.
Because we are measuring acceleration directly we do not need an observer. This means (24) can take the form of

$$u_{ad} = u_{nn} = M^T \sigma\left(N^T \varphi\right) \ . \tag{25}$$

M and *N* are the network weights based on the directly measured state. We also use the error dynamics from Equation (25), which are of the form

$$\begin{aligned} \dot{E} &= \overline{A}E + Kz \\ z &= \overline{C}E \end{aligned} \ . \tag{26}$$

In our case,

$$\overline{A} = A_1 - B_1 D_c C_1 \quad , \tag{27}$$

where the gain K is chosen to satisfy the basic stability law $\overline{A} - K\overline{C}$. Now the network weights can be calculated:

$$\begin{aligned} \dot{M} &= -\Gamma_M \left[\left(\hat{\sigma} - \hat{\sigma}' N^T \varphi \right) E^T P \overline{b} + kM \right] \\ \dot{N} &= -\Gamma_N \left[\varphi E P \overline{b} M^T \hat{\sigma}' + kN \right] \end{aligned} , \tag{28}$$

in which Γ_M and $\Gamma_N > 0$ are positive definite adaptation gain matrices, $k > 0$ is a σ- modification constant and $\hat{\sigma}'$ is the Jacobian computed at each estimate.

4.0 Wind Tunnel Models

4.1 Model Construction

Typically, subsonic wind tunnel models are manufactured from stainless steel or other hard materials to ensure rigidity of the parts of the model not under study. The main requirement of our wind tunnel model is that the portion of the model forward from the empennage has to be as close to rigid as possible while allowing the aeroelastically scaled empennage to be fully attached to the model. From our previous experience in tail buffet alleviation with the F-15, our lab has been successful in creating subsonic wind tunnel models that meet this requirement by modifying commercially available airplane kits. For our F/A-18 model, we purchased a 1/12th scale model kit from JD Enterprises (http://www.jdenterprise.net), and its dimensions are shown in Table 1.

Table 1: Dimensions of the Modified F/A-18 Model

Length	63 inches (5 feet 3 inches)
Wing span, shortened	~29+ inches (2 feet 5+ inches)
Weight approx. (*empty*)	28 lb
Scale	1/12th scale

Our first step in the construction process was to have a structure to stiffen the fuselage. A wing box/fuselage skeleton was designed and constructed by the Aerospace machine shop. This steel structure is basically a wing box assembly with attachment points in the rear for the empennage to be attached, a plate on the bottom for stinger mounting bracket to be attached, and a T beam welded to the front which extended to the nose. The wings are bolted to the wing box by means of three bolts in each wing. Aluminum washers in the shape of the root airfoil are sandwiched between the inside of the fiberglass skin and the body stiffening structure; their primary purpose is for local stiffening and to bear the root loads. As a result, the rigidity of the wings is increased to a great enough extent as to not see any response from them in a random excitation of the entire model when measured at the vertical tails. The specifications of the F-18 aircraft model are given in Table 1. The fuselage is made of epoxy fiberglass, with glass encapsulated foam core wings, area ruled exhaust duct with intake ducting and all wood parts are factory precut and finished Before we can perform wind tunnel testing we needed to calculate reduced frequency. For proper scaling, the reduced frequency should be the same for the model and the actual aircraft. The equation is of the form,

$$R = \frac{f \times c}{U_\infty} \quad , \qquad (29)$$

where
f: frequency
c: characteristic length
U_∞: air stream speed.

Buffeting occurs when the dynamic pressure is approximately 340 psf on the actual full-scale F-18. Using a reference density at 12,000 ft, U1 is found to be 201.17 m/s (660.04 ft/s). Since our model is 1/12 scale, the ratio of characteristic lengths is 1/12. A typical value for test dynamic pressure in the Georgia Tech Research Institute (GTRI) MTF wind tunnel is between 5 to 15 psf, where U∞ is 66.5 to 115.3 ft/s and subsonic M=0.059 to 0.102 (although values of q up to 45 psf

are possible). We choose 12 psf (= 103.1 ft/s) as our dynamic pressure for our frequency calculations.

$$\frac{f_{model}}{f_{actual}} = \frac{U_{\infty,model}}{U_{\infty,actual}} \times \frac{c_{actual}}{c_{model}} = \frac{31.42 \text{ m/s}}{201.17 \text{ m/s}} \times 12 = 1.8742 \quad . \tag{30}$$

As determined, the frequencies are presented in Table 2.

Table 2: Frequencies of F/A-18 and Model

Mode number	Actual F/A-18 Frequency (Hz)	Model Frequency (Hz)	Calculated Model frequencies (Hz)
1st Bending	16.73	30.57	31.2851
1st Torsion	46.77	85.46	87.4599

The horizontal and vertical tails were manufactured at Georgia Tech in the composites lab. They were a fiber/matrix mixture of a synthetic cloth with 0 to 90° woven fibers and bondo resin with hardener. The original tails were made with approximately 11 layers or fiber. A vacuum process was used. We started with a layer of cloth, resin was applied to completely saturate the cloth, and then another layer was applied and the process was continued until we reached the desired thickness. We laid the wet sample across a metal plate with a hole at the base and a plastic airtight cover on top. Excess air and matrix was drawn out, and the sample was left to set overnight. The horizontal tails had a metal rod inserted at mid-span for stiffening purposes and for a means of connection to the empennage assembly. Large metal masses were added to the underside of the horizontal tails so that their dynamic response could not be confused with the vertical tails. The structure of the empennage consists of nine pairs of aluminum rings to simulate engine cavities, which help support the vertical and horizontal tails. These rings are 1/2 inch long and 2/16 inch thick. The centers of the paired rings are spaced 3.25 inches apart and each pair is separated 1 inch from the adjacent pair. Composite strips above and below reinforce the rings and simulate the rib structure in the actual F/A-18. These rings are bolted inside two 13.5-inch long C-braces. A metal brace is bolted to the top surface of the C-brace. The composite vertical tails are bolted on to these braces. A V-shaped plate is bolted to the assembly at about 70 percent of the C-brace's length. It serves as one of the connections for the horizontal tail. The horizontal tail is mounted by means of a three-point connection using three rods. These three rods, parallel to the elastic axis, were installed in each horizontal tail during the layup of the lamina before curing in an autoclave. The free ends of these rods were threaded to allow installation through the vertical tail C-bracket and fastened by threaded nuts. The other two connections are to the C-brace bolt holes which are shared by a pair of rings. One end of the C-brace is bolted to a metal plate. This metal plate is bolted to the back end of the body stiffening structure discussed earlier. The empennage is installed to the back of the wing box with eight hex bolts. The fiberglass skin is cut into pieces and attached with threaded fasteners. This overall design allows for the model to be disassembled and reassembled at any time and allows parts to be changed out. Once the empennage had been assembled adjustments were made to get the dynamic response of the vertical tails. Figure 11 through Figure 16 show the results.

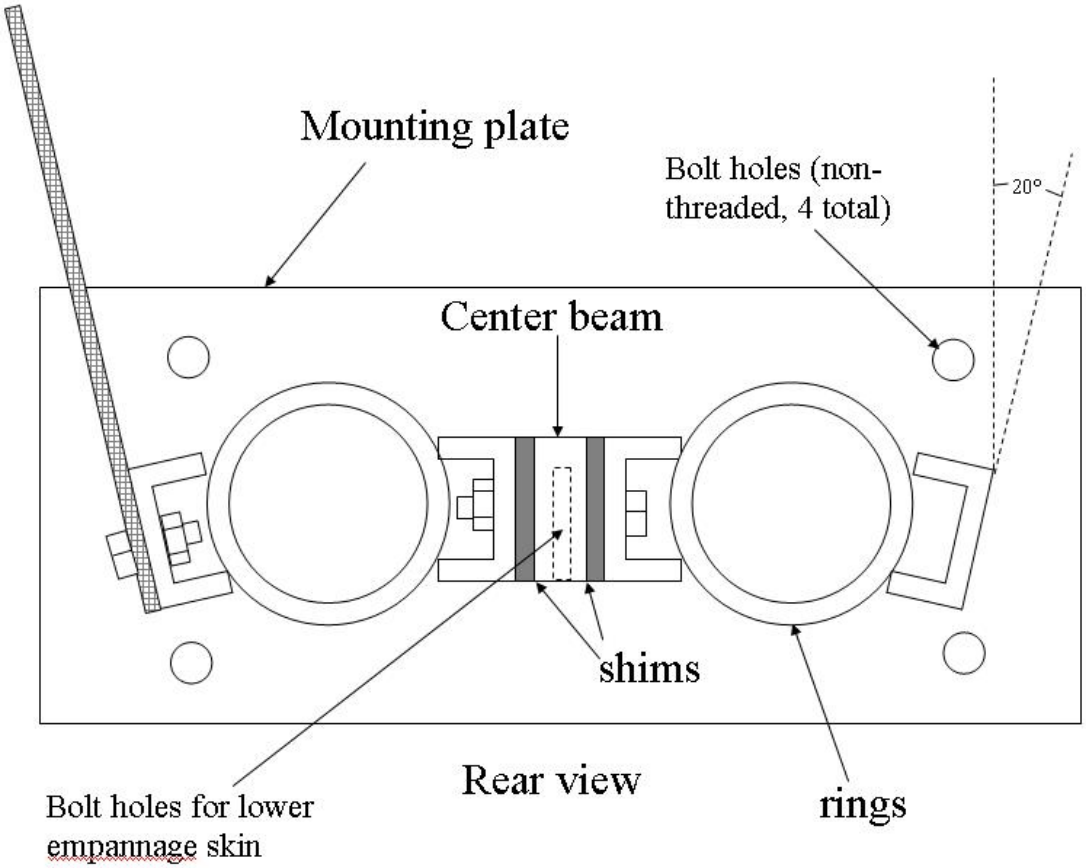

Figure 11: F/A-18 Wind Tunnel Model Empennage Design Rear View

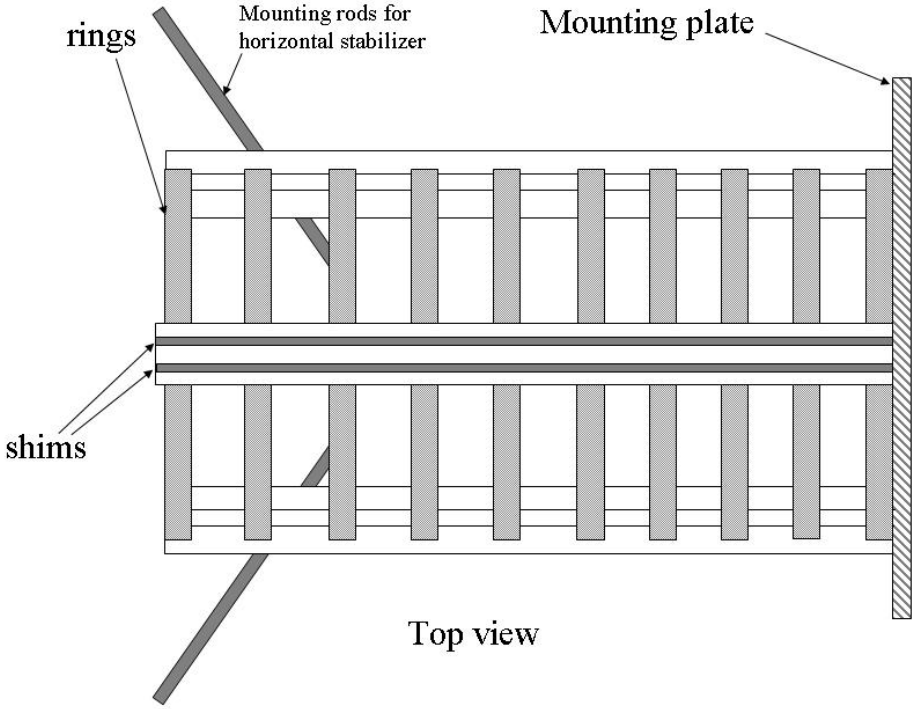

Figure 12: F/A-18 Wind Tunnel Model Empennage Design Top View

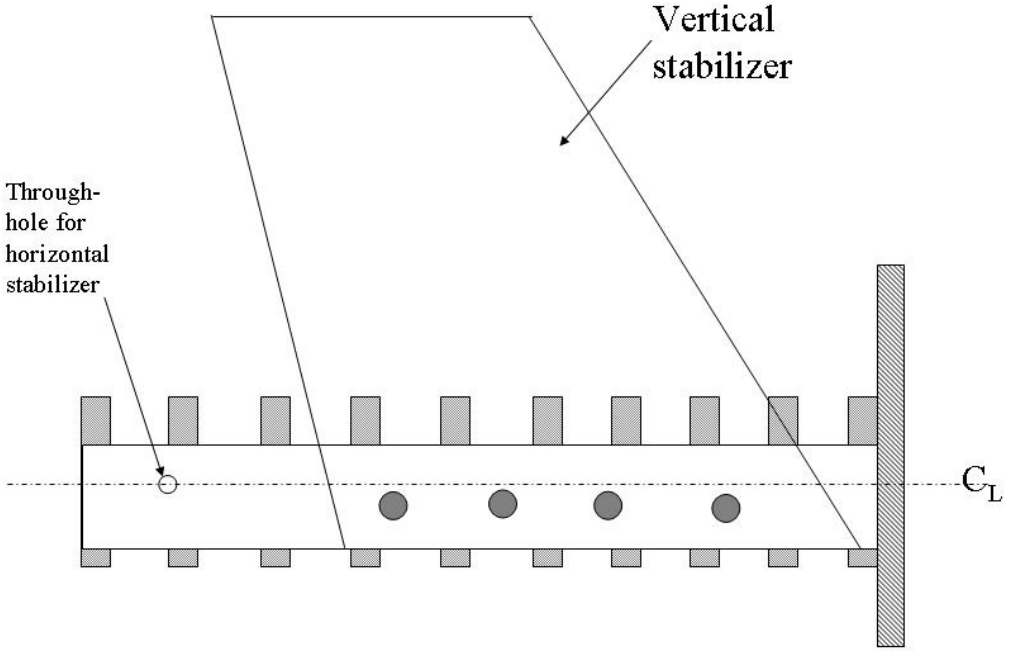

Figure 13: F/A-18 Wind Tunnel Model Empennage Design Side View

Figure 14: F/A-18 Wind Tunnel Model Empennage and Testing Fixture

Once the empennage had been tested, it was installed into the fuselage.

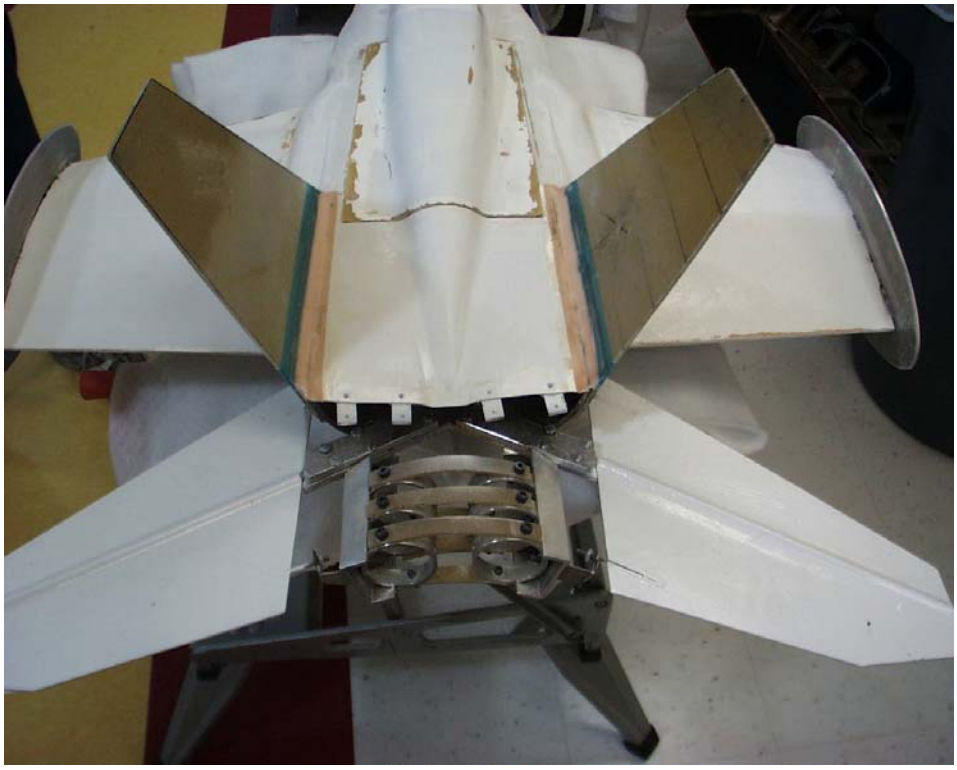

Figure 15: F/A-18 Wind Tunnel Model Empennage Installation

Figure 16: Final F/A-18 Wind Tunnel Model without OPSAs

4.2 Wind Tunnel Testing

The wind tunnel used is GTRI's model test section (MTF) closed return, subsonic wind tunnel. The cross-sectional dimensions of this tunnel are $43^{3/8}$ inches wide by $30^{3/8}$ inches tall. The usable length of the tunnel is 90 inches. Due to the length of the model and the desired 32° of AOA (worst-case scenario), the model must be mounted from the side of the tunnel to clear the walls when pitched to higher AOA. This is acceptable as this test is not measuring forces and moments through the balance. The full wing span of the original model is 48 inches, which is too large for the wind tunnel test section width. Therefore, 9 inches will be removed from the wing at each wing tip, and the wing will span the 30-inch width of the test section. To abate any vortices that would be created from 3-D lifting wing tip geometries after wing shortening, a symmetric oval end plate was attached to the new wing tips. Previous experiments have shown that the vortex produced by the leading edge extensions of the wing breaks down before the vertical tail at angles of 25° (worst case being 32°) and is maximum at Mach number of 0.3 (see Figures 17, 18, and 19).

Figure 17: F/A-18 Wind Tunnel Model Mounting Structure, AOA 35°

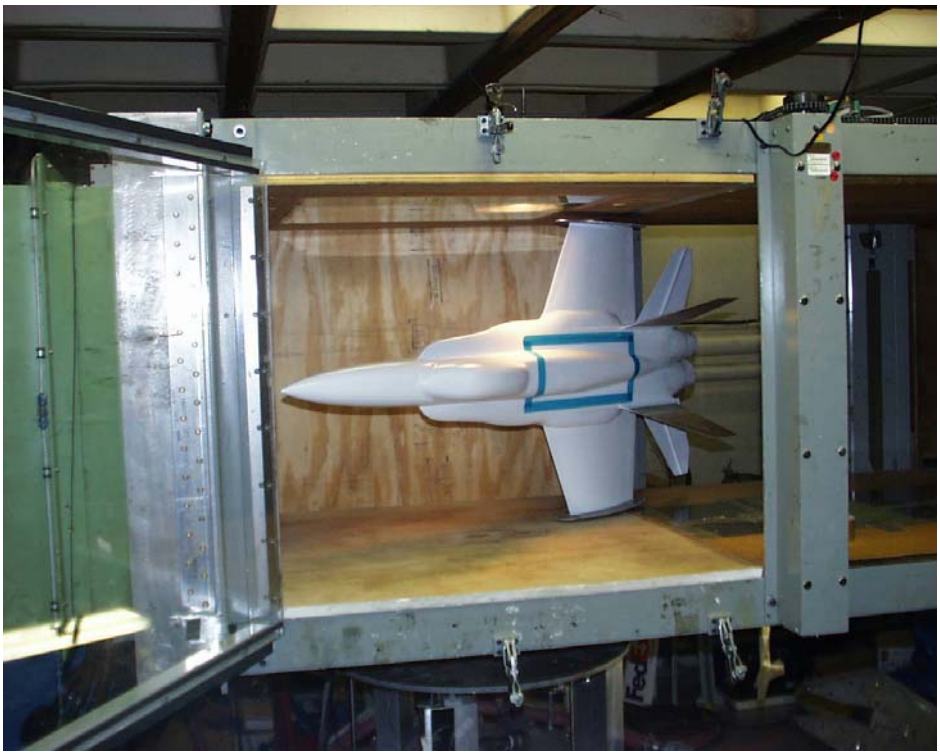

Figure 18: F/A-18 Wind Tunnel Model Mounted at 35° AOA

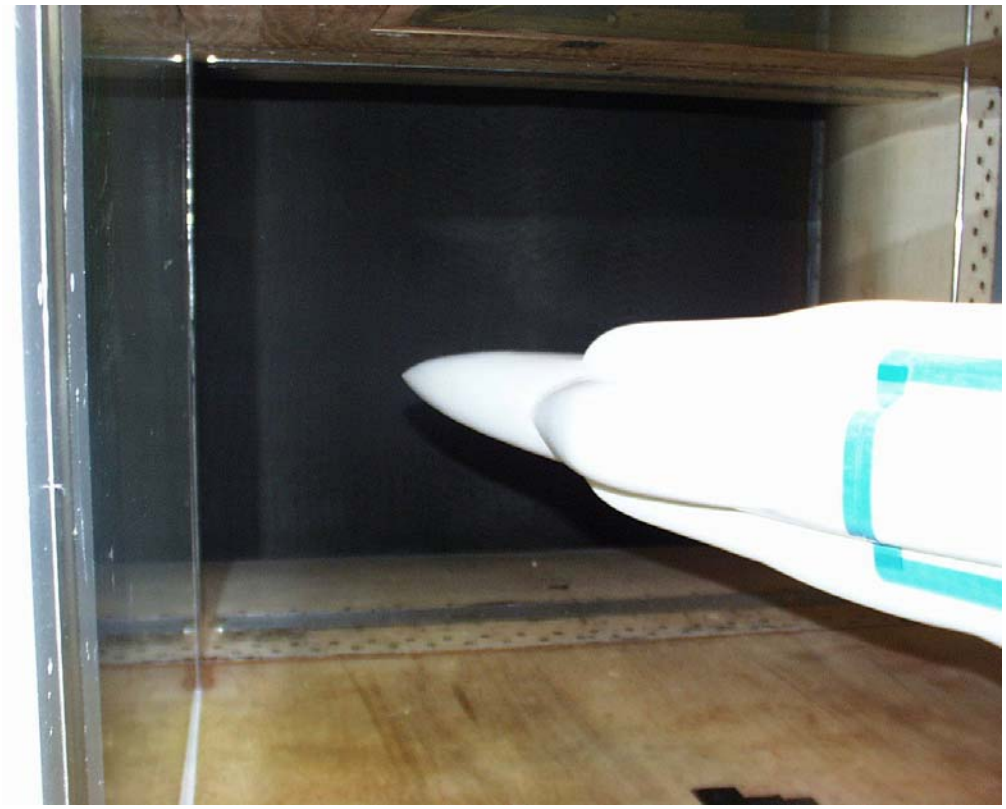

Figure 19: F/A-18 Wind Tunnel Model Mounted at 35° AOA Showing Nose Clearance

4.3 Phase I: Model Validation

As the wind tunnel model is not a standard test article for wind tunnel testing, it must be validated to verify if it can produce the correct flow field at the different test conditions. To obtain the required flow visualization two types of tufts were used: 1) 2-inch tufts mounted with tape along the port wing leading edge, along the fuselage at the port wing root, on the fuselage between the vertical tails, and 2) a single tuft on a long metal rod which can be moved to locations around the model. The tuft on this rod is approximately 6 inches long and has been marked with a red marker in a segmented fashion to help visualize the flow. Specifically, this test validated that the proper vortex is created from the leading edge extension (LEX), and as AOA and q is increased, the vortex bursts and causes tail buffet. The test conditions are shown in Table 3.

Table 3: Verification Test Conditions

AOA (degrees)	Dynamic Pressure (q) psf
0	**5**
0	**12**
20	**5**
20	**12**
25	**12**
30	**5**
30	**9**
30	**12**
30	**15**
32	**12**
35	**12**

The testing clearly showed a well-defined vortex starting at the LEX. As the AOA is increased, the vortex interaction with the vertical tails causes the vertical tails to visibly vibrate. As the AOA is increased the burst point of the vortex moves forward and is ahead of the vertical tails. At 35° AOA the vibrations reduce slightly which was an indication that we had the maximum tail buffet effect at 32° AOA. A dynamic pressure of 15 psf was not attempted at 35° AOA as the amount of blockage was a concern in this wind tunnel. Movies of each test were made which includes narrative and can be sent upon request. These movies clearly show the vortex interaction with the fuselage and the vertical tails.

4.4 Phase II: Open Loop Characterization of the Plant in the Wind Tunnel

Once Phase I proved that we had a valid wind tunnel model, we needed to characterize the tail buffet effect. Specifically, we need to find the exact worst-case buffet conditions in the open loop case. This both confirms the worst-case buffet condition and helps to determine the amount of control authority the control scheme will need. This involves installing the OPSAs, as seen in the Figures 20 and 21.

To obtain maximum effectiveness to suppress the magnitude of the vibrations, we used two OPSAs for each targeted mode, one mounted on each side of the vertical tail. The targeted modes

will be the first bending and first torsion modes. The actuators used will be those that were successfully used on the F-15 wind tunnel model, which, in that case, controlled the third mode. These OPSAs used a P-810.10 stack which has a maximum blocked force of 50 Newtons.

From Ashley's report[13], the elastic axis of the vertical tail is found to be at 45 percent of chord. This was located and drawn on the starboard vertical tail on the model. The inboard OPSA was installed on this elastic axis at the root of the tail. The outboard OPSA was installed along the elastic axis directly opposite the inboard bending OPSA. Originally an ethyl cyanoacrylate adhesive, which is a fast bonding, single-component adhesive was used to bond the actuators. This adhesive failed when the OPSAs were activated. This was replaced by a silicon-based adhesive which has a 24- to 72-hour cure time. To control this first torsion mode, the two torsion OPSAs were installed 45° from the elastic axis.

Adjustment in dynamic pressure, q, and subsonic Mach number, M, in the ranges specified in the table below. Time domain data was collected for 60 seconds for each run, and an auto power spectra is determined at a later time. From previous experiments with the F/A-18, a single sensor was placed on the upper trailing tip of the starboard vertical tail. This sensor is a PCB accelerometer of 100 mV/g sensitivity.

The equipment that was used during the wind tunnel tests included the following:

- 1 PCB 352-A24 accelerometer with their PCB 480-D06 signal conditioners
- 1 Krohn-Hite Model 3343 analog filter unit used as an anti-aliasing filter
- 1 Pentium-based PC for controller design and data postprocessing. The software and input/output (I/O) board are built by Quanser which uses MATLAB® 6.

At a free stream dynamic pressure of 12 psf, the AOA is varied from 0 to 25° in 2° increments. Above 25°, the tested AOAs are 30, 32, and 35°. This shows how the effect of the vortex increases with AOA. This testing clearly shows the worst-case buffet condition is at 32° AOA, which corresponds to the full-scale aircraft and previous work by others.

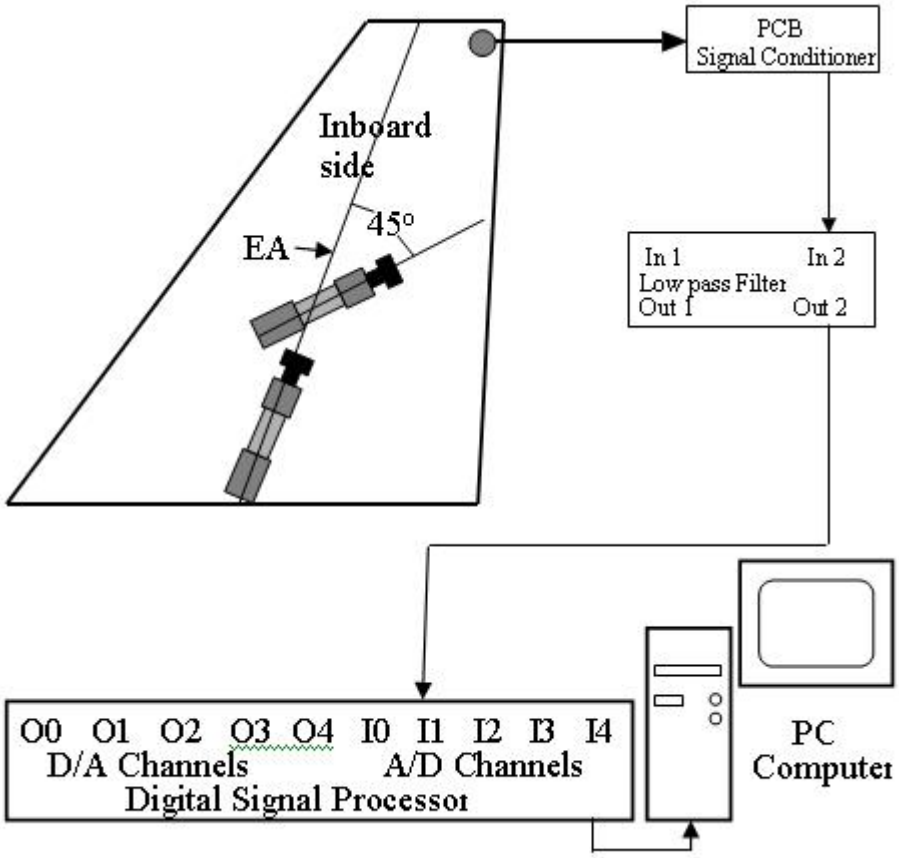

Figure 20: Schematic of Inboard OPSA Installation on Starboard Vertical Tail

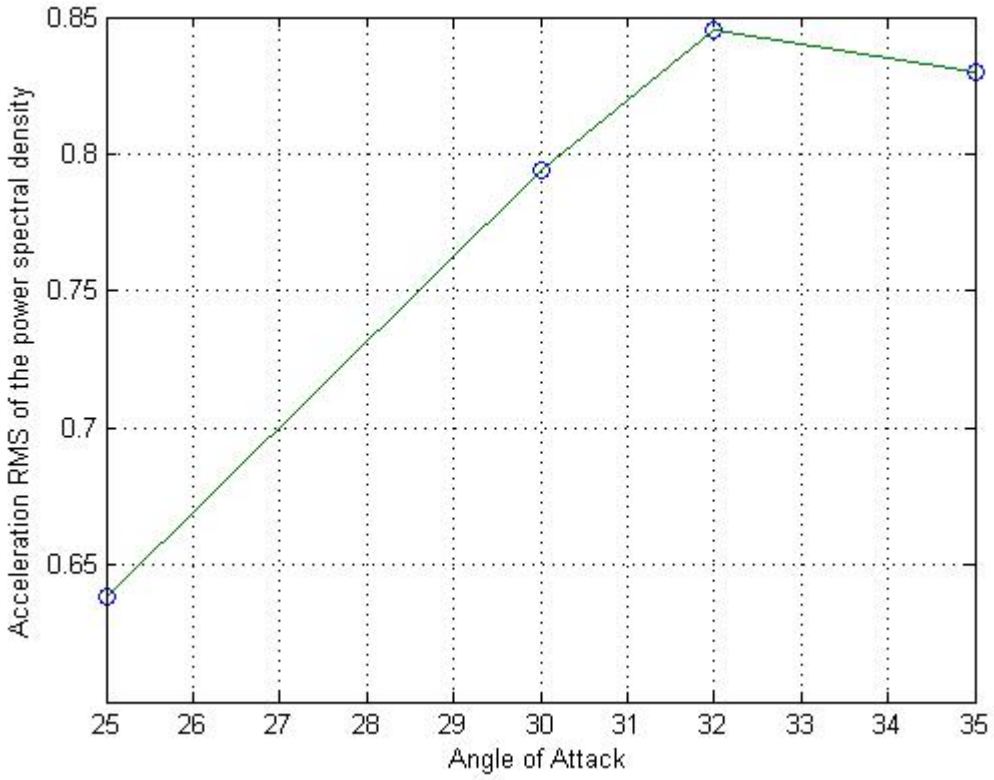

Figure 21: RMS of Acceleration with OPSAs Installed at q = 12 psf

In measuring the first bending mode frequency at 25° AOA q of 5 psf and 35° AOA q of 12 psf, we see the first bending frequency at 38.6 Hz and 36.1 Hz, respectively. This shows that as the tail buffet effect increases, the modal frequency changes by approximately 3 Hz. If a linear controller is tuned to control at the q = 0 psf of 39.05 Hz, it will be less effective at higher speeds and higher AOA.

4.5 Phase III: Closed Loop Control of the Plant Using Linear Acceleration Feedback Controller in the Wind Tunnel

Because the first bending mode is dominant and the first resonant frequency, we will design the controller to control this mode. On the F/A-18 model, we experimentally obtained the transfer function, coherence, and frequency response between the inboard bending OPSA and the sensor by using a random excitation of a bandwidth of 0 to 150 Hz.

Parameters appear in Table 4, controller parameters appear in Table 5, and inboard bending information appears in Figures 22 and 23.

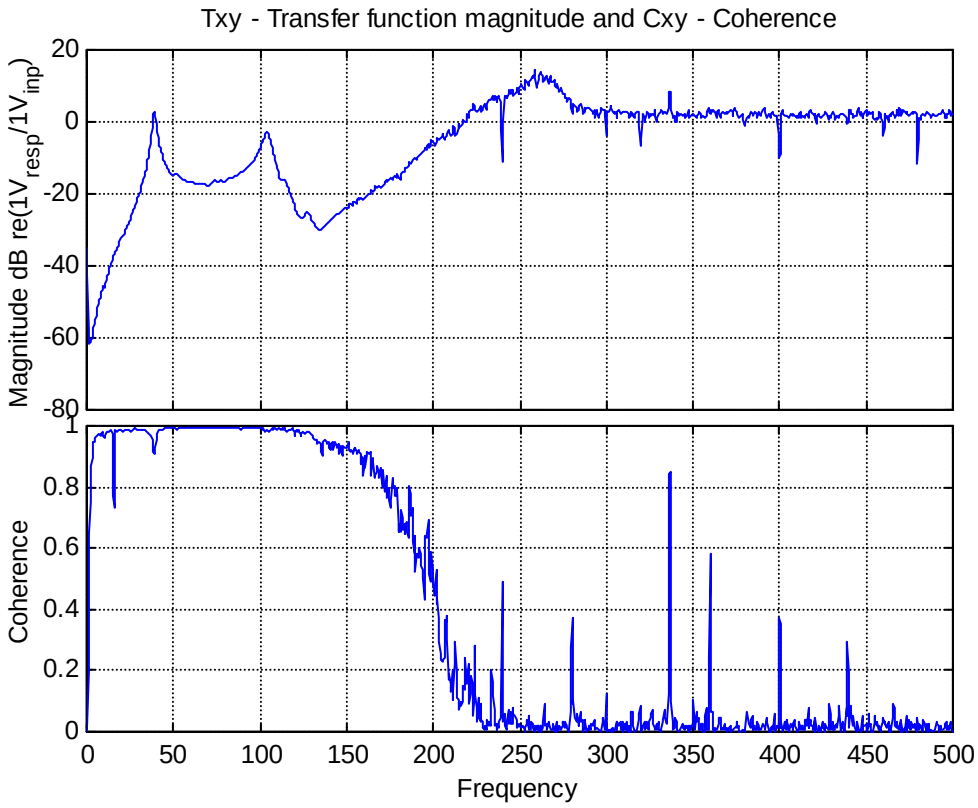

Figure 22: Transfer Function and Coherence between Inboard Bending OPSA and Sensor

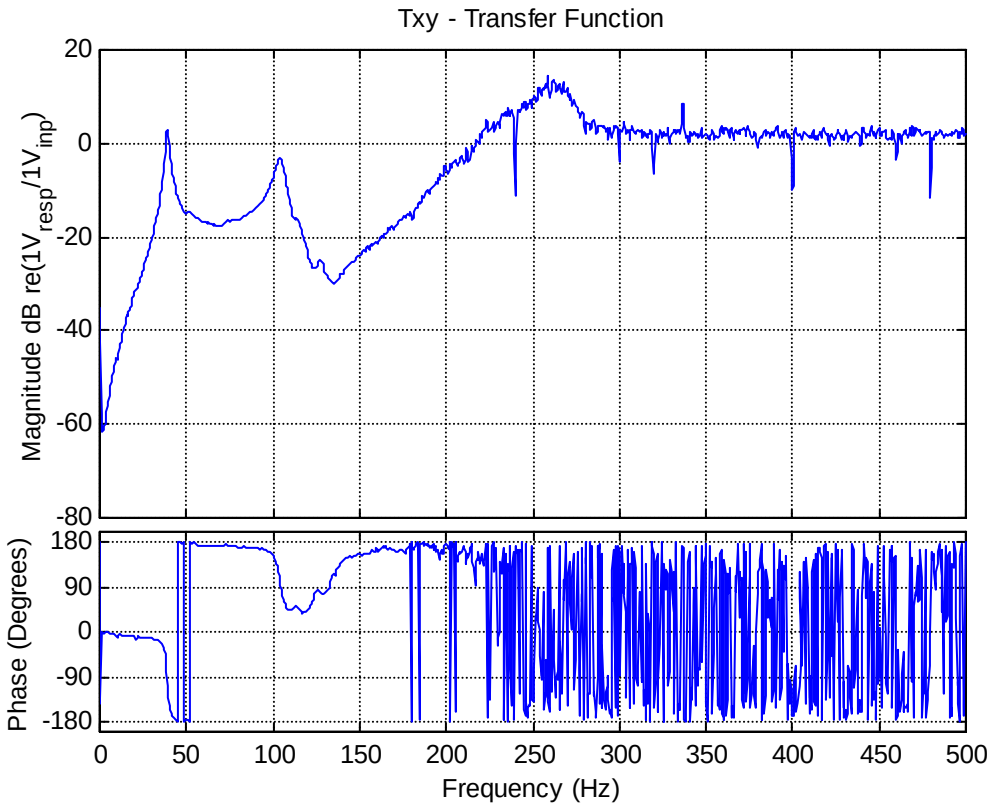

Figure 23: Frequency Response Function between Inboard Bending OPSA and Sensor

Table 4: Experimental Open Loop Parameters

Mode	Frequency (Hz)	Damping Ratio (ξ_1-percent)
1st Bending Mode	38.834	2.463
1st Torsion Mode	103.683	2.620

Table 5: Designed Linear Controller for F/A-18 Vertical Stabilizer

Controller Parameters		
Frequency f_c (Hz)	Damping Ratio (ξ_c-percent)	Gain γ
38.834	88.178%	-10.7

4.6 Control Authority Assessment

To perform a control authority assessment, the PSDs of the open loop vibrations at different free stream velocities and the random excitation will be compared. The AFC control scheme is shown in Figure 25.

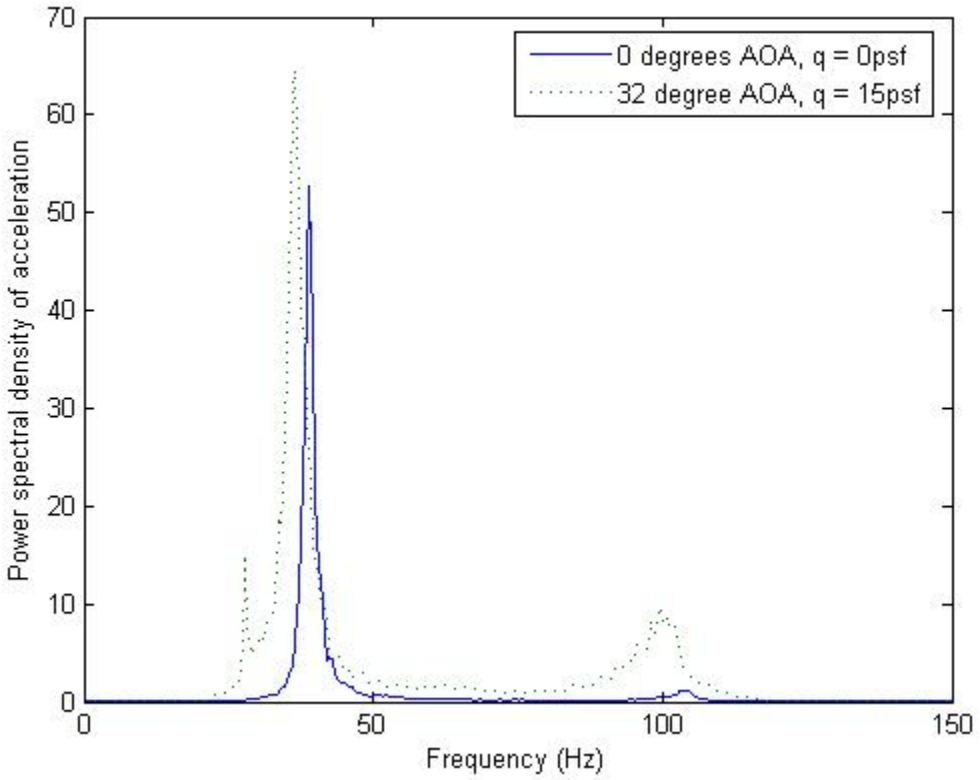

Figure 24: Control Authority Assessment of the AFC Control Scheme

In Figure 25, we see the magnitude of the open loop response at the worst case buffet condition (α=32°, q = 15 psf) and the response of the tail when a random excitation is passed through the inboard bending OPSA (α=0°, q = 0 psf). Both cases are measured by the same accelerometer as mentioned before. Two items are clearly visible in this graph: 1) the current control scheme does not have enough power to completely control the vibration at worst case, and 2) the frequencies shift as the AOA and free stream velocity increase. An ANN has shown to be a valid solution to control a system whenever there are parameter changes.

4.7 Phase IV: Closed Loop Control of the Plant Using Linear AFC Augmented with an ANN in the Wind Tunnel

With the development of an AFC with an ANN, a controller should provide sufficient control authority across a wide range of AOA. The neural network would supplement the tuned acceleration feedback controller by actively adjusting the plant model as the AOA changed. This will actively adjust the controller range of optimal authority as the flight condition changed increasing its adapting to local environments.

In tail buffet alleviation, we typically control distinct modes of the structure. To begin the development of the neural network augmented control for tail buffet, we will start with converting the following plant (31a) and controller (31b) equations into state space:

$$\begin{cases} \ddot{q}_1 + 2\xi_1\omega_1 q_1 + {\omega_1}^2 q_1 = -n_s^1\,\bar{a}_{11}\gamma_1{\omega_{c1}}^2\eta_1(t) + \bar{f}_1(t) \\ \ddot{\eta}_1(t) + 2\xi_{c1}\omega_{c1}\dot{\eta}_1(t) + {\omega_{c1}}^2\eta_1(t) = \bar{b}\ddot{q}_1 \end{cases} . \qquad (31a, b)$$

The plant is as follows:

$$A_{mi} = \begin{bmatrix} 0 & 1 \\ -\overline{\omega}_{si}^2 & -2\zeta_{si}\overline{\omega}_{si} \end{bmatrix} . \qquad (32)$$

$$B_{mi} = \begin{bmatrix} 0 \\ 1 \end{bmatrix}$$

$$C_{mi} = \begin{bmatrix} -\overline{\omega}_{si}^2 & -2\zeta s_i\overline{\omega}_{si} \end{bmatrix}$$

$D_{mi} = 1$

C_m is set to give acceleration as an output which simulates the sensor installed on the tail. We will use a reference model in the following form:

$$A_{1i} = \begin{bmatrix} 0 & 1 \\ -\overline{\omega}_{si}^2 & -2\zeta_{si}\overline{\omega}_{si} \end{bmatrix} \qquad (33)$$

$$B_{1i} = \begin{bmatrix} 0 \\ 1 \end{bmatrix}$$

$$C_{1i} = \begin{bmatrix} -\overline{\omega}_{si}^2 & -2\zeta s_i\overline{\omega}_{si} \end{bmatrix}$$

$D_{1i} = 1$.

For the controller the state space model becomes

$$A_{ci} = \begin{bmatrix} 0 & 1 \\ -\omega_{ci}^2 & -2\zeta_{ci}\omega_{ci} \end{bmatrix} \qquad (34)$$

$$B_{ci} = \begin{bmatrix} 0 \\ \bar{b} \end{bmatrix}$$

$$C_{ci} = \begin{bmatrix} 1 & 0 \end{bmatrix}$$

$D_{ci} = 0$

5.0 Conclusions

This research program developed a systematic procedure to design the OPSA and the controller parameters, placement of sensors and actuators, to control buffet-induced vibrations. The program designed for the OPSA parameters and specified the number of piezoelectric stacks for an ideal performance level. Open loop preparation tests of a $1/12^{th}$ scale F/A-18 vertical tail model subjected to buffet loads were conducted in the GTRI's MTS closed return, subsonic wind tunnel that verified that buffet vortices could be generated.

An analytical model was developed that demonstrated that the tail buffet-induced vibrations on the F/A-18 can be controlled using acceleration feedback control and ANN-based controllers. The theoretical studies showed that it is possible to obtain the required control authority for tail buffet alleviation by using piezoceramic stack-based actuators, by designing an effective linear control scheme, by optimal placement of sensors and actuators on the vertical tail, and by augmenting the linear controller with an ANN to control changes in response due to parameter changes.

A $1/12^{th}$ scale model was built of an F/A-18 based on a kit that was commercially available. The model was then modified to meet structural rigidity requirements for the wind tunnel while maintaining the aeroelastic requirements for the vertical tail section. The wing span was reduced from 48 inches to 30 inches to fit in the test section. Experimental validation of the theoretical results was limited to open loop preparation tests of the model. No closed loop data were obtained by the end of the contract. It is recommended that the wind tunnel experiment using the $1/12^{th}$ scale model be conducted and the results compared to full-scale vertical fin buffet data. From this data, estimates of fatigue life could be made showing the effectiveness of the active control system. Results would also be used to identify system scaling issues that would affect its implementation.

Before implementing the system in an operational F/A-18 and performing flight tests, it is suggested that wind tunnel tests be conducted on other models and the full scale aircraft to characterize any parameter changes. The response data from these experiments would be used to simulate, improve, and optimize the control of displacements and accelerations in the vertical tail both with the linear controller and the ANN controllers. Additional research should also include controller designs for dynamic maneuver loading and nonlinear response for large deformations.

6.0 References

1. Fung, Y.C., An Introduction to the Theory of Aeroelasticity, Dover Publications, Inc., 1955, pp. 52-55.
2. Balas, M.J., "Active Control of Flexible Systems," *J. of Optimization Theory and Applications*, Vol. 25, No. 3, 1978, pp. 415-436.
3. Goh, C.J. and Caughey, T.K., "On the stability problem caused by tailite actuator dynamics in the collocated control of large space structures," *Int. J. of Control*, Vol. 41, No. 3, 1985, pp. 787-802.
4. Juang, J.N. and Phan, M., "Robust Controller Designs for Second-Order Dynamic Systems: A Virtual Passive Approach," *J. of Guidance, Control and Dynamics*, Vol. 15, No. 5, 1992, pp. 1192-1198.
5. Nikzad, K. and Ghaboussi, J., "Application of multi-layered feedforward neural networks in digital vibration control," Proceedings of the IJCNN – International Joint Conference on Neural Networks, 1992, p. 1004.
6. Preumont, A., Dufour, J.P., and Malekian, C., "Active Damping by a Local Force Feedback with Piezoelectric Actuators," *J. of Guidance, Control and Dynamics*, Vol. 15, No. 2, 1992, pp. 390-395.
7. Bean, D. E., Greenwell, D. I., and Wood, N. J., "Vortex control technique for the attenuation of fin buffet," *Journal of Aircraft*, Vol. 30, No. 6, November-December, 1993, pp. 847-853.
8. Drakunov, S. V., Ozguner, U., and Lenning, L., "Use of neural networks and sliding modes in vibration damping," Proceedings of SPIE - The International Society for Optical Engineering, Vol. 1919, 1993, pp. 174-181.
9. Pado, Lawrence E. and Jacobs, Jack H., "Hybrid cascading neural network for modeling fighter aircraft buffet pressures," Intelligent Engineering Systems Through Artificial Neural Networks, Vol. 3, 1993, pp. 877-884.
10. Rock, S., Ashley, H., Digumarthi, R., and Chaney, K., "Active control for fin buffet alleviation," AIAA Guidance, Navigation and Control Conference, Monterey, CA; 9-11 August 1993. pp. 1051-1056, 1993 AIAA PAPER 93-3817.
11. Sim, E. and Lee, S.W., "Active Vibration Control of Flexible Structures with Acceleration Feedback," *Journal of Guidance*, Vol. 16, No. 2, 1993, pp. 413-415.
12. Ferman, M.A., Liguore, S.L., Smith, C.M., and Colvin, B.J., "Composite Exoskin Doubler Extends F-15 Vertical Tail Fatigue Life," 34th Structures, Structural Dynamics, and Materials Conf., Vol. 1, 1993, pp. 398-407.
13. Ashley, H., Rock, S.M., Digumarthi, R., Channey, K., and Eggers, A.J., "Active Control for Fin Buffet Alleviation," WL-TR-93-3099, 1994.
14. Jacobs, J.H., Hedgecock, C.E., Lichtenwalner, P.F., Pado, L.E., and Washburn, A.E., "Use of artificial neural networks for buffet environments," *Journal of Aircraft*, Vol. 31, No. 4, July-August 1994, pp. 831-836.
15. Kandil, Osama A.; Massey, Steven J.; and Kandil, Hamdy A., "Computations of vortex-breakdown induced tail buffet undergoing bending and torsional vibrations," Collect Tech Papers AIAA/ASME/ASCE/AHS Struct Struct Dyn Mater, No. 2, 1994, pp. 977-992.
16. Hebbar, S.K., Platzer, M.F., and Frink, W.D., "Effect of Leading-Edge Extension Fences on the Vortex Wake of an F/A-18 Model," *Journal of Aircraft*, Vol. 32, No. 3, 1995, pp. 680-682.

17. Lazarus, K.B., Saarmaa, E., and Agnes, G.S., "Active smart material system for buffet load alleviation," Proc. SPIE, Vol. 2447, 1995, pp. 179-192.
18. Long, T.W., Hanzevack, E.L., and Caggiano, S., "Noncolocated vibration control using neural networks," IEEE International Symposium on Intelligent Control - Proceedings, 1995, pp. 9-14.
19. Goh, C.J. and Yan, W.Y., "Approximate Pole Placement for Acceleration Feedback Control of Flexible Structures," *J. of Guidance*, Vol. 19, No. 1, 1996, pp. 256-259.
20. Hauch, R.M., Jacobs, J.H., Ravindra, K., and Dima, C., "Reduction of vertical tail buffet response using active control," *J. of Aircraft*, Vol. 33, No. 3, 1996, pp. 617-622.
21. Lichtenwalner, P.F., Little, G.R., Pado, L.E., and Scott, R.C., "Adaptive neural control for active flutter suppression," American Society of Mechanical Engineers, Fluids Engineering Division (Publication) FED, Vol. 242, Proceedings of the ASME Fluids Engineering Division, 1996, pp. 3-8.
22. Lichtenwalner, P.F., Little, G.R., and Scott, R.C., "Adaptive neural control of aeroelastic response," Proceedings of SPIE - The International Society for Optical Engineering, Vol. 2717, 1996, pp. 199-209.
23. Lu, Z., Shi, X., Wang, X., and Xu, M., "Active structure vibration control using dynamic neural networks: modeling error, nonlinear, parameter imprecise and disturbance," American Society of Mechanical Engineers, Design Engineering Division (Publication) DE, Vol. 93, Active Control of Vibration and Noise, 1996, pp. 363-370.
24. Moore, J.W., Spangler, R.L., Lazarus, K.B., and Henderson, D.A., "Buffet load alleviation using distributed piezoelectric actuators," Industrial and Commercial Applications of Smart Structures Technologies, ASME, AD Vol. 52, 1996, pp. 485-490.
25. Neural networks and their applications, edited by J.G. Taylor, Chichester; New York: UNICOM; Wiley, 1996.
26. Pado, Lawrence E., Damle, and Rajendra R., "Predictive neuro control of vibration in smart structures," Proceedings of SPIE - The International Society for Optical Engineering, Vol. 2715, 1996, pp. 567-575.
27. Varadan, V.V., Young-Hun, L., and Varadan, V.K., "Closed Loop Finite-Element Modeling of Active/Passive Damping in Structural Vibration Control," *J. of Smart Materials and Structures*, Vol. 5, No. 5, 1996, pp. 685-694.
28. Young, J.W. and Hansen, C.H., "Control of Flexural Vibration in Stiffened Structures using Multiple Piezoceramic Actuators," *Applied Acoustic*, Vol. 49, No. 1, 1996, pp. 17-48.
29. Wang, T.C. and Sinha, A., "Neural network based control of vibration in the presence of uncertainties in system parameters and excitation frequencies," American Society of Mechanical Engineers, Design Engineering Division (Publication) DE, Vol. 93, Active Control of Vibration and Noise, 1996, pp. 339-345.
30. Zhou, K., Doyle, C.D., and Glover, K., "Robust and Optimal Control," Prentice-Hall, 1996.
31. Moses, R.W., "Vertical-tail-buffeting alleviation using piezoelectric actuators: some results of the actively controlled response of buffet-affected tails (ACROBAT) program," Proc. SPIE, Vol. 3044, 1997, pp. 87-98.
32. Nitzsche, F., Zimcik, D.G., and Langille, K., "Active control of vertical fin buffeting with aerodynamic control surface and strain actuation," 38th AIAA/ASME/ASCE/AHS/ASC Structures, Structural Dynamics, and Materials Conference, Vol. 2, 1997, pp. 1467-1477.
33. Preumont, A., "Vibration Control of Active Structures: An Introduction," Kluwer Academic Publishers, 1997.

34. Redmond, J. and Barney, P., "Vibration Control of Stiff Beams and Plates Using Structurally Integrated PZT Stack Actuators," *J. of Intelligent Material Systems and Structures*, Vol. 8, 1997, pp. 525-535.
35. Seeman, W., Wolf, K.D., Straub, A., Hagedorn, P., and Chang, F.," Bonding Stresses Between Piezoelectric Actuators and Elastic Beams," Proceedings of SPIE, Vol. 3041, 1997, pp. 665-675.
36. Bayon de Noyer, M., and Hanagud, S., "Comparison of H2 optimized design and cross-over point design for acceleration feedback control," Collect Tech Pap, Struct. Struct. Dyn. Mater. Conf., Vol. 4, 1998, pp. 3250-3258, AIAA-98-2091.
37. Hopkins, M.; Henderson, D.; Moses, R.; Ryall, T.; Zimcik, D.; and Spangler, R.,"Active vibration suppression systems applied to twin tail buffeting," Proc SPIE Int Soc Opt Eng, Vol. 3326, 1998, pp. 27-33.
38. Pado, Lawrence E., Lichtenwalner, Peter F., Liguore, Salvatore L.; and Drouin, Donald, "Neural predictive control for active buffet alleviation," Proceedings of SPIE - The International Society for Optical Engineering, Vol. 3326, 1998, pp. 47-57.
39. Spencer, M.G., Sanner, R.M., and Chopra, I., "Adaptive neurocontroller for vibration suppression and shape control of a flexible beam," *Journal of Intelligent Material Systems and Structures*, Vol. 9, No. 3, March 1998, pp. 160-170.
40. Bayon de Noyer, M., and Hanagud, S, "Single Actuator and Multi-Mode Acceleration Feedback Control," *J. of Intelligent Material Systems and Structures*, Vol. 9, No. 7, 1999, pp. 522-545.
41. Bayon de Noyer, Maxime P., Roberts, P.J.; and Hanagud, S.V., "Active damping by acceleration feedback control and redistribution of stresses in the structure," American Society of Mechanical Engineers, Aerospace Division (Publication) AD, Vol. 59, 1999, pp. 373-380.
42. Hanagud, S., de Noyer, M. Bayon; Luo, H.; Henderson, D.; and Nagaraja, K.S., "Tail buffet alleviation of high performance twin tail aircraft using piezo-stack actuators," Collection of Technical Papers - AIAA/ASME/ASCE/AHS/ASC Structures, Structural Dynamics and Materials Conference, Vol. 2, 1999, pp. 1054-1064.
43. Manser, R.; Simpson, J.; Becker, J.; Duerr, J.; Floeth, E.; Herold-Schmidt, U.; Stark, H.; and Zaglauer, H.W., "Fin-buffet alleviation via distributed piezoelectric actuators: Full scale demonstrator tests," Proc SPIE Int Soc Opt Eng, Vol. 3674, 1999, pp. 13-21.
44. Moses, R.W., "Contributions to active buffeting alleviation programs by the NASA Langley Research Center," AIAA Paper 99-1318, April 1999.
45. Nitzsche, F.; Zimcik, D.G.; Ryall, T.G; Moses, R.W.; and Henderson, D.A., "Control law synthesis for vertical fin buffeting alleviation using strain actuation," AIAA Paper 99-1317, April 1999.
46. Pado, L.E. and Lichtenwalner, P.F., "Neural predictive control for active buffet alleviation," Collection of Technical Papers AIAA/ASME/ASCE/AHS/ASC Structures, Structural Dynamics and Materials Conference, Vol. 2, 1999, pp. 1043-1053.
47. Spangler, R.L. and Jacques, R.N., "Testing of an active smart material system for buffet load alleviation," 40th AIAA/ASME/ASCE/AHS/ASC Structures, Structural Dynamics, and Materials Conference, 1999, AIAA-99-1317.
48. Suleman, Afzal; Costa, Antonio P.; and Moniz, Paulo A., "Experimental °utter and buffeting suppression using piezoelectric actuators and sensors," Proc SPIE Int Soc Opt Eng, Vol. 3674, 1999, pp. 72-81.

49. Nitzsche, F., et al., “Finite Element Approach for Design Control algorithms for Vertical Fin Buffeting using Strain Actuation,” Pre-print, NATO Active Control Technology Conference, Braunschweig, Germany, May 2000.
50. P. Roberts and S. Hanagud, "Model based simulation of the Active damping of a Cantilever Plate and Redistribution of Stresses," Adaptive Structures and Material Systems, ASME, 2000.
51. Bayon De Noyer, and Maxime P., Tail buffet alleviation of high performance twin tail aircraft using offset piezoceramic stack actuators and acceleration feedback control, Thesis (Ph.D.), School of Aerospace Engineering, Georgia Institute of Technology, 2000.
52. Kandil, O.A., Yang, Z., and You, R., "Effectiveness of adaptive flow control for twin-tail buffet," AIAA Applied Aerodynamics Conference, 18th, Denver, CO; 14-17 August 2000, pp. 714-724, 2000 AIAA Paper 2000-4414.
53. Scott, Robert C., "Active control of wind-tunnel model aeroelastic response using neural networks," Proceedings of SPIE - The International Society for Optical Engineering, Vol. 3991, 2000, pp. 232-243.
54. Appa, K., Ausman, Khot, J.N.S., and Brenner, M. J., "Buffet load alleviation using a smart actuation system," AIAA-2001-1665 AIAA/ASME/ASCE/AHS/ASC Structures, Structural Dynamics, and Materials Conference and Exhibit, 42nd, Seattle, WA, April 16-19, 2001.
55. Burnham, J.K.; Pitt, D.M.; White, E.V.; Henderson, D.A.; and Moses, R.W., "An advanced buffet load alleviation system," 42nd AIAA/ASME/ASCE/AHS/ASC Structures, Structural Dynamics, and Materials Conference and Exhibit Technical Papers, Vol. 5, 2001, pp. 3579-3588.
56. El-Badawy, A.A. and Nayfeh, A.H., "Buffet alleviation of twin-tailed fighter aircraft using saturation-based control," Proc Int Modal Anal Conf IMAC, Vol. 2, 2001, pp. 928-934.
57. El-Badawy, A.A. and Nayfeh, A.H., "Use of linear and nonlinear vibration absorbers for buffet al.leviation of twin-tailed fighter aircraft," Proc SPIE Int Soc Opt Eng, Vol. 4326, 2001, pp. 397-407.
58. Flynn, G.A., Morrison, J.F., and Mabey, D.G., "Buffet alleviation on swept and unswept wings at high incidence," *Journal of Aircraft*, Vol. 38, No. 2, March/April, 2001, pp. 368-378.
59. Hanagud, S.; Lu, X.; Roberts, P.; and Henderson, D., "Model based simulation of buffet-induced vibration control of a F/A-18 vertical stabilizer," Collection of Technical Papers - AIAA/ASME/ASCE/AHS/ASC Structures, Structural Dynamics and Materials Conference, Vol. 2, 2001, pp. 1279-1288.
60. Jha, R. and He, C., "Design and experimental validation of adaptive neuro-controller for beam vibration suppression using piezoelectric actuators," American Society of Mechanical Engineers, Aerospace Division (Publication) AD, Vol. 64, 2001, pp. 271-281.
61. Nitzsche, F., Moses, R.W., Zimcik, D.G., Ryall, T.G., and Henderson, D.A., "Closed-loop control tests for vertical fin buffeting alleviation using strain actuation," *Journal of Guidance*, Control, and Dynamics, Vol. 24, No. 4, pp. 855-857, July-August 2001.
62. M. Sharma and A.J. Calise, "Neural Network Augmentation of Existing Linear Controllers," in AIAA Guidance, Navigation and Control Conference, 2001.
63. Sheta, E.F.; Harrand, V.J.; and Huttsell, L.J., "Active vortical flow control for alleviation of twin-tail buffet of generic fighter aircraft," Journal of Fluids and Structures, Vol. 15, No. 6, pp. 769-789, August 2001.

64. Hanagud, S., Bayon de Noyer, M., Luo, H., Henderson, D., and Nagaraja, K.S., "Tail buffet alleviation of high-performance twin-tail aircraft using piezostack actuators," *AIAA Journal*, Vol. 40, No. 4, April 2002, pp. 619-627.
65. Ghee, Terence A., Gonzalez, Hugo A., and Findlay, David B., "Tail buffet alleviation through the use of wing-strake fillet shapes," *Journal of Aircraft*, Vol. 39, No. 1, January/February 2002, pp. 100-108.
66. Becker, J. and Luber, W., "The role of buffeting the structural design of eurofighter," Collect Tech Pap AIAA ASME ASCE AHS Struct Struct Dyn Mater., Vol. 6, 2003, pp. 4449-4458.
67. Bong-Jun Yang, Naira Hovakimyan, and Anthony J. Calise, “Output Feedback Control of an Uncertain System using an Adaptive Observer,” in IEEE Conference on Decision and Control, Maui, HI, pp. 1705-1710, December 2003.
68. Bong-Jun Yang, Naira Hovakimyan, Anthony J. Calise, and James I. Craig, “Experimental Validation of an Augmenting Approach to Adaptive Control of Uncertain Nonlinear Systems,” in AIAA Guidance, Navigation and Control Conference, No. AIAA-2003-5715, Austin, TX, 2003.
69. Hanagud, S., Patel, U., Roberts, P., and Henderson, D., "Control authority and the design of active controllers for buffet suppression," Collection of Technical Papers - AIAA/ASME/ASCE/AHS/ASC Structures, Structural Dynamics and Materials Conference, Vol. 2, 2003, pp. 1081-1091.
70. Sheta, E.F. and Huttsell, L.J., "Characteristics of F/A-18 vertical tail buffeting," *Journal of Fluids and Structures*, Vol. 17, No. 3, 2003, pp. 461 - 477.
71. Sheta, Essam F., "A multidisciplinary analysis of tail buffeting alleviation using streamwise fences," *Journal of Vibration and Control*, Vol. 9, No. 5, 2003, pp. 583–604.
72. Sheta, E.F.; Moses, R.W.; Huttsell, L.J.; and Harrand, V.J., " Active control of F/A-18 vertical tail buffeting using piezoelectric actuators," 44th AIAA/ASME/ASCE/AHS/ASC Structures, Structural Dynamics, and Materials Conference, Vol. 6, 2003, pp. 4427-4437.
73. Ferman, M.A., Huttsell, L.J., and Turner, E.W., "Experiments with tangential blowing to reduce buffet response on an F-15 model," *Journal of Aircraft*, Vol. 41, No. 4, July/August 2004, pp. 903-910.
74. Sheta, Essam F., "Alleviation of Vertical Tail Buffeting of F/A-18 Aircraft," *Journal of Aircraft*, Vol. 41 No. 2, 2004, pp. 322-330.
75. Polytec PI www.polytecpi.com.
76. Demuth, H. and Beale, M., "Neural Network Toolbox User's Guide," The Mathworks Inc., 1992-2001.

LIST OF ACRONYMS, ABBREVIATIONS, AND SYMBOLS

ACRONYM	DESCRIPTION
ACROBAT	actively controlled response of buffet affected tails
ACSM	active control surface modal
ANCAR	adaptive neural control of aeroelastic response
ANN	adaptive neural network
AOA	angle of attack
AOFA	adaptive output feedback augmentation
BACT	benchmark active controls technology
BLA	buffet load alleviation
CPU	computational processing unit
DANNC	direct adaptive neural network controller
FEM	finite element model
GTRI	Georgia Tech Research Institute
HCNN	hybrid cascading neural network
LQR	linear quadradic regulator
MIMO	multi-input/multi-output
MLP	multilayer Perceptron
MTF	model test section
NPC	neural predictive control
OPSA	offset piezoceramic stack actuator
PID	proportional integral derivative
PSD	power spectral density
PZT	piezoceramic actuator - lead zirconate titanate
RVDT	rotational variable displacement transducer
RMS	root mean squared
SISO	single-input/single-output
TCB	tangential central blowing
TSB	tangential spanwise blowing
TVB	tangential vortex blowing
TDT	transonic dynamics tunnel